JCI insight

Distinct transcriptional and epigenomic programs define Hofbauer cells in term placenta

Benjámin R. Baráth, Dóra Bojcsuk, Krisztian Bene, Noemí Caballero-Sánchez, Tímea Cseh, João CR. de Freitas, Petros Tzerpos, Marta Toth, Zhonghua Tang, Seth Guller, Zoárd Tibor Krasznai, Patrícia Neuperger, Gabor J. Szebeni, Gergely Nagy, Tamás Deli, Laszlo Nagy

JCI Insight. 2025. https://doi.org/10.1172/jci.insight.195801.

Resource and Technical Advance | In-Press Preview | Immunology | Reproductive biology

Graphical abstract

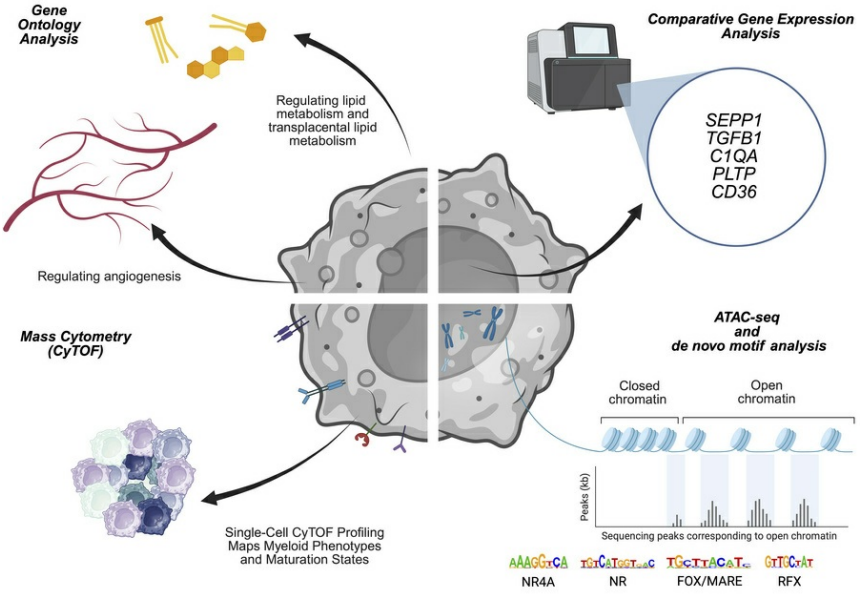

Find the latest version:

https://jci.me/195801/pdf

Distinct Transcriptional and Epigenomic Programs Define Hofbauer Cells in Term Placenta

Benjámin R. Baráth[1,2,3], Dóra Bojcsuk[1], Krisztian Bene[1,3], Noemí Caballero-Sánchez[1,2], Tímea Cseh[1], João CR. Freitas[3], Petros Tzerpos[1], Marta Toth[4], Zhonghua Tang[5], Seth Guller[5], Zoárd Tibor Krasznai[6], Patrícia Neuperger[7], Gábor J. Szebeni[7,8], Gergely Nagy[1], Tamás Deli[6], and Laszlo Nagy[1,3,9]

[1] Department of Biochemistry and Molecular Biology, Faculty of Medicine, University of Debrecen, Debrecen, Hungary;

[2] Doctoral School of Molecular, Cell and Immunobiology, University of Debrecen, Debrecen, Hungary;

[3] Institute for Fundamental Biomedical Research, Johns Hopkins All Children's Hospital St. Petersburg, FL, USA

[4] Department of Immunology, Faculty of Medicine, University of Debrecen, Debrecen, Hungary

[5] Department of Obstetrics, Gynecology and Reproductive Sciences, Yale School of Medicine, New Haven, CT, USA.

[6] Department of Obstetrics and Gynecology, Faculty of Medicine, University of Debrecen, Debrecen, Hungary;

[7] Laboratory of Functional Genomics, Core Facility, HUN-REN Biological Research Centre, Szeged, Hungary;

[8] Department of Internal Medicine, Hematology Centre, Faculty of Medicine, University of Szeged, Szeged, Hungary;

[9] Departments of Medicine, Pediatrics, Physiology, Pharmacology and Therapeutics and Biomedical Engineering, Johns Hopkins University School of Medicine, Baltimore, MD, USA

Authorship notes: B.R.B. and D.B. contributed equally to this work.

Conflict of interest: The authors have declared that no conflict of interest exists.

Address correspondence to: Laszlo Nagy, Johns Hopkins All Children's Hospital, 600 Fifth Street South, St. Petersburg, Florida, 33701, USA. Phone: 1.727.767.8928; Email: lnagy@jhmi.edu.

ABSTRACT

Hofbauer cells (HBC) are fetal-derived macrophages located in the placenta that contribute to antimicrobial defense, angiogenesis, tissue remodeling, and metabolic processes within the chorionic villi. Although their roles in placental biology are increasingly recognized, the mechanisms that regulate HBC identity and function are not yet fully defined. This study aimed to define the core transcriptomic and epigenomic features of HBCs in term placentas and to examine their capacity for transcriptional responsiveness and phenotypic variation. Using chromatin accessibility profiling and bulk RNA sequencing, we found that HBCs exhibit a unique gene expression and chromatin accessibility profile compared to other fetal and adult macrophages. We identified a coordinated transcriptional network involving nuclear receptors NR4A1–3, the glucocorticoid receptor (GR), and RFX family members (RFX1, RFX2, RFX5) that appears to shape HBC identity, particularly through pathways linked to lipid metabolism and angiogenesis. Although exploratory in nature, *in vitro* stimulation studies showed that HBCs exhibited increased transcriptional activity in response to combined IL-4 and RSG treatment, including induction of the lipid transporter CD36. Mass cytometry analysis revealed surface markers indicative of both immature and mature macrophage states. Together, these results indicated that HBCs represent a distinct and diverse macrophage population with specialized and adaptable regulatory program in the human placenta.

GRAPHICAL ABSTRACT

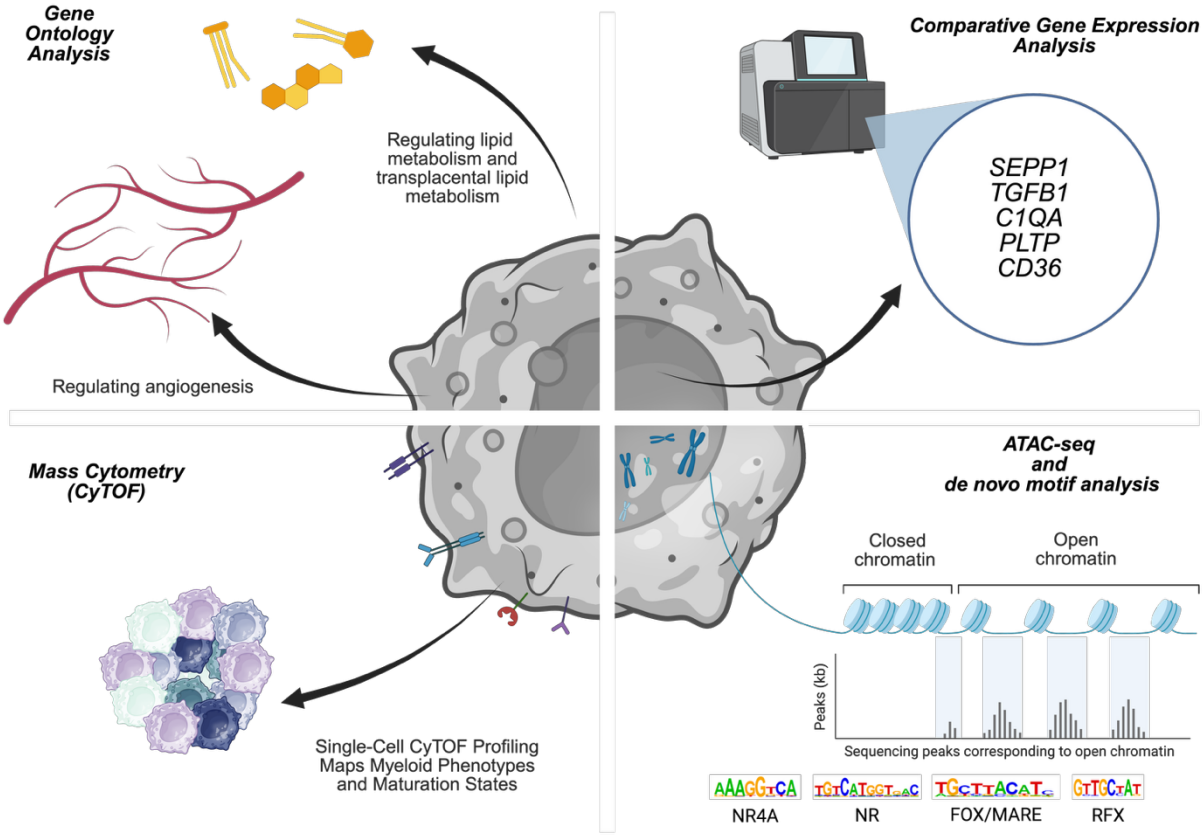

INTRODUCTION

Macrophages are a heterogeneous population of immune cells of myeloid origin that constantly fine-tune their functional state and that of surrounding cells in response to changes in the tissue environment (1). Macrophages originate from erythroid-myeloid progenitors (EMPs) or hematopoietic stem cells (HSCs), with tissue-specific resident macrophages primarily derived from yolk sac-derived EMPs during development (2) and HSC-derived macrophages recruited later in life associated with aging, diseased or chronic inflammatory states, etc. Lineage-determining transcription factors (LDTFs), along with other signals from the surrounding cell niche, drive cell type-specific tissue-resident macrophage differentiation during organogenesis. However, the specific signals and mechanisms inducing and maintaining tissue macrophage identity and function have to be determined for each macrophage subtype.

The human placenta is a transient yet essential and highly versatile organ, playing a vital role in the progression of pregnancy. It forms a vital interface between the mother and fetus, facilitating the transport of oxygen, nutrients, and waste products, while also producing hormones crucial for pregnancy and fetal development. It performs these functions through its highly specialized microarchitecture and a distinct, placenta-specific set of cells. Fetal-derived placental macrophages, also known as Hofbauer cells (HBCs), are large (10-30 μm in diameter) vacuolated and granulated cells found in the chorionic villi of the placenta (3, 4) in proximity to villous endothelial cells, fibroblasts, and the different subtypes of trophoblasts (TBs). Functional and gene expression studies have shown that HBCs exhibit a high level of phagocytosis and play an essential role in protecting against pathogens, placental morphogenesis, e.g., vasculogenesis, angiogenesis, maintaining placental tissue homeostasis (5–8). The latest findings suggest that HBCs are derived from placental erythromyeloid precursors (PEMPs) throughout pregnancy, with no apparent monocyte-derived

supplementation under homeostatic conditions (9). We refer to previously written articles focusing on HBCs in various pregnancy complications (7, 8, 10, 11).

The limited epigenetic studies available on HBCs shed light on their origin and the mechanism underlying the differences in Human Leukocyte Antigen – DR isotype (HLA-DR) expression of HBCs during pregnancy. Thomas and colleagues reported that while first-trimester HBCs lack HLA-DR expression, third-trimester HBCs exhibit variable HLA-DR levels. Additionally, HBC DNA methylation profiles remain consistent throughout pregnancy, suggesting negligible monocyte contribution (9). Methodological advances in recent years have made it possible to study cellular heterogeneity at the fetal-maternal interface (12–14). Due to the structural and physiological differences between humans and other species, the relevance of animal models, especially mouse models, is often debated in the context of reproductive research focusing on the human placenta. There is one intriguing study that found a transcriptomic correlation between mouse placental macrophages, human HBCs, and microglia cells, suggesting that HBCs could serve as a biomarker for brain damage susceptibility (15).

Complications such as preeclampsia, villitis of unknown etiology (VUE), fetal growth restriction, and preterm labor are frequently associated with abnormalities in placental vascular development, inflammation, and disruptions in maternal-fetal immune regulation, processes in which HBCs are thought to contribute. However, the regulatory networks that define HBC identity, function, and phenotype under physiological conditions remain incompletely understood. To address this gap, we performed a systematic molecular characterization of primary HBCs isolated from uncomplicated term placentas. Using an integrative multi-omics approach, including bulk RNA sequencing (RNA-seq), Assay for Transposase-Accessible Chromatin sequencing (ATAC-seq), Cytometry by Time-of-Flight (CyTOF), and *in vitro* stimulation experiments, we sought to define the transcriptional and chromatin accessibility

landscape of HBCs and assess their potential for regulatory responsiveness and phenotypic variation. This approach provides a foundational step toward characterizing the transcriptional and regulatory landscape of purified HBCs in late gestation and may serve as a useful reference for future investigations into placental immune function and related pathologies.

RESULTS

Purification and phenotypic characterization of term HBCs

Five eligible term placentas (n = 5) were collected, each within 20 minutes of elective cesarean section performed without labor at the University of Debrecen, Department of Obstetrics and Gynecology (Table 1). HBCs were isolated using negative selection for CD10 and EGFR, then sorted based on CD163 expression as described previously (Table 2) (7). Prior to CD163 sorting, 70-80% of the cells showed typical pleomorphic macrophage morphology with characteristic granular, vacuolar, and foamy cytoplasm. In the remaining 20-30%, we detected large, contaminating cells (data not shown; Figure 1A). The contamination got reduced upon sorting down to approximately 10% (Figure 1B, Supplementary Figure 1B). Our gating strategy used for FACS is depicted in Supplementary Figure 1. Our single-cell RNA-seq supports the macrophage identity of our isolates (Supplementary Figure 2). Considering the possibility of contamination with maternal decidua macrophages, we benefited from the presence of male newborns (n=3), which allowed us to estimate the percentage of impurity by tracking the extent of female material through sex-specific genes. Analyzing X-linked gene expression (i.e., X Inactive Specific Transcript [*XIST*] expression), we estimated the potential contamination to be between 2-9% (Supplementary Table 1). The purity of the isolation was further supported by the PCA plot comparing our isolates to maternal decidual and placental macrophage of first and trimester (Supplementary Figure 3) (13, 16) The high-yield isolation

of HBCs allowed us to ask questions regarding the molecular characteristics, such as global gene expression, of this distinct cell type.

HBCs have a distinct gene expression landscape compared to other fetal and adult macrophages

Next, we focused on the gene expression (bulk RNA-seq) profile of isolated HBCs and compared them to 15 different fetal and adult monocyte and macrophage subpopulations, such as adult Kupffer cells (KC) (17), monocyte-derived macrophages (MDM) (18), alveolar macrophages (AM) (19), adult microglia (aMG) (20), fetal microglia (fMG) (21), fetal liver macrophage (fLM) (21), mononuclear and multinucleated osteoclasts (MoOC, and MuOC) (22), osteoclast precursors (OCP) (23), spleen (SpM) (24), intestinal (IM) (25), and skin macrophages (SkM) (26), as well as spleen (SMo) (24), blood monocytes (BMo) (24) and cord blood monocytes (CBMo) (27). Multidimensional scaling of RNA-seq data revealed that all samples of HBC populations clustered together rather tightly, and they appear to be distinct from other healthy fetal and adult macrophage populations (Supplementary Figure 4A). For further, more in-depth analysis, we only kept those cell types that had a fetal counterpart (CBMo, aMG, fMG, KC and fLM, as well as those whose transcriptional regulation we later examined together with that of the HBCs (AM and MDM; Figure 2A). These comparisons showed that the HBC populations from our donors are similar to each other with little patient-to-patient variability as far as their global gene expression is concerned, and that HBCs' gene expression profile is distinct, as they showed to be clustered far from other fetal and adult macrophage populations. Moreover, HBCs displayed a distinct gene expression profile, clustering far from other fetal and adult macrophage populations. The low inter-sample variability is also illustrated by the correlation plot with Pearson correlation values in Supplementary Figure 4B and the sample-to-sample distance heat map in Supplementary

Figure 4C. This raises, at least formally, the question of whether these cells meet the criteria for being *bona fide* macrophages.

To support the claim that the isolated cells were indeed macrophages, we used a list of macrophage-specific transcription factors and plotted the average expression of the top 30 genes encoding these factors (Figure 2B) (28). HBCs show high levels of expression genes encoding these factors (i.e., Transcription Factor PU.1 [*PU.1*], Y-Box Binding Protein 1 [*YBX1*], certain basic helix-loop-helix proteins such as Hypoxia Inducible Factor 1 Subunit Alpha [*HIF1A*], Inhibitor of DNA Binding 2 [*ID2*], and Upstream Transcription Factor 2 [USF2], as well as Activating Transcription Factor 3 [*ATF3*] and 4 [*ATF4*], and Interferon Regulatory Factor 8 [*IRF8*]); in addition, the essential macrophage marker Colony Stimulating Factor 1 Receptor (*CSF1R*) is also expressed at a high level in HBCs, further establishing that the isolated cells are indeed macrophages. This comparison also shows key differences in the relative expression of these genes when HBCs are compared to other fetal and adult macrophage subpopulations. For example, HBCs express CCAAT-Enhancer-Binding Protein delta (*CEBPD*) as opposed to *CEBPA*, which is highly enriched in microglia, and *CEBPB*, which is expressed primarily in AMs, KCs, and MDMs. Figure 2C highlights the high expression of genes that are considered as HBC marker genes within the context of fetal-maternal interface (29).

Distinct gene expression pathways are enriched in HBCs

Since gene expression analysis verified the purity and identity of the isolated cells as fetal macrophages, we considered the different biological processes regulated by transcription in HBCs. We systematically compared the bulk RNA-seq profiles obtained from HBCs, CBMo, aMG, fMG, AM, MDM, KC, and fLM and identified 20 gene clusters representing 13,866 differentially expressed genes (DEGs; Figure 2D, top). Additionally, we found 8,423 genes

expressed at similar levels (no significant statistical difference between the groups) in all these cell types (Figure 2D, bottom). Clusters C1–C5 contained genes enriched in HBCs, with Cluster 1 (C1) being primarily HBC-dominant, while Clusters 2–5 (C2, C3, C4, C5) also showed considerable expression in other cell types. CD36, HIF1A, Selenoprotein P (*SEPP1*), Colony Stimulating Factor 1 Receptor (*CSF1R*), Complement C1q A chain and C chain (*C1QA* and *C1QC,* respectively), V-Set and Immunoglobulin Domain Containing 4 (*VSIG4*), Phospholipid Transfer Protein (*PLTP*) and the HBC marker Folate Receptor Beta (*FOLR2*) are all genes that are highly expressed in HBCs and are found in Cluster 1. Highly expressed genes in C2-C5 include *CCL4, CCL3, CXCL8 CD163, CD14, IL1B*, and Fibronectin 1 *(FN1)*. Among the genes showing absolute HBC specificity are H19 Imprinted Maternally Expressed Transcript (*H19*), Delta Like Non-Canonical Notch Ligand 1 (*DLK1*), Tachykinin Precursor 1 and 3 (*TAC1* and *TAC3*, respectively), Insulin-Like Growth Factor 2 (*IGF2*), Isthmin 2 (*ISM2*), Chorionic Somatomammotropin Hormone 1 and 2 (*CSH1* and *CSH2*), Apolipoprotein L Domain Containing 1 (*APOLD1*), Insulin-Like Growth Factor Binding Protein 1 (*IGFBP1*), and Pappalysin 2 (*PAPPA2*; Figure 2E). In addition, the 1,518 genes of Cluster 1 are enriched in pathways related to tissue and embryo morphogenesis, heart and skeletal muscle development, epithelial cell proliferation, and Vascular Endothelial Growth Factor A – Vascular Endothelial Growth Factor Receptor 2 (*VEGFA-VEGFR2*) signaling controlling angiogenesis (Supplementary Figure 4D). In order to compare tissue macrophage functions in a more systematic and potentially functional manner, we have took curated gene sets representing key macrophage sensing and effector functions such as cellular fitness, extracellular milieu, metabolism, nuclear receptors, the detection of and response to microorganisms as outlined by Lazarov and colleagues (Figure 3A) (30), and compared the expression of these key gene sets along with genes responsible for angiogenesis (derived from the PANTHER Pathways dataset). As shown on Figure 3A, HBCs are distinct in having higher

expression levels of angiogenetic, extracellular milieu, cellular fitness, and nuclear receptor signaling genes. Example genes for these functions are depicted in Fig 3B, Supplementary Figure 5 and Supplementary Figure 6. There is a lower expression of genes associated with the response to microbes and metabolism. Despite the low ranking of metabolism, genes playing role in lipid metabolism and transport are highly represented in C1 and C2 (e.g. *CD36*, *PLTP*, and Acyl-CoA Synthetase Long Chain Family Member 1 [*ACSL1*]). Nuclear receptor signaling and lipid metabolism regulation are functionally linked: Nuclear Receptor Subfamily 4 Group A (*NR4A*) genes, Peroxisome Proliferator Activated Receptors (*PPARs*), Retinoid X Receptor Alpha (*RXRA*), and Glucocorticoid Receptor (*GR*) are enriched in HBCs (Figure 3B, C). Given the prior *in vitro* demonstration of HBC dexamethasone (DEX) responsiveness by Tang Z et al. (31), we investigated GR-associated gene sets in this cell type, finding that the majority of DEX-responsive genes with nearby GR binding sites show higher expression in HBCs compared to the other examined cell types (Figure 3D) (32). Importantly, the expression of the nuclear receptor PPAR-regulated scavenger and the fatty acid receptor *CD36* is particularly high in HBC, suggesting a key role for this latter molecule (Figure 2D, Figure 3E). Finally, given the low ranking of the antimicrobial function on Figure 3A, we assessed whether HBCs represent a cell type already committed to one of the prototypic macrophage polarization paradigms (M1 or M2). Examining a set of selected polarization markers (33–36), we found that HBCs show mixed polarization phenotype having high expression levels of genes of certain M1 (C-C Motif Chemokine Ligand 3 and 4 [*CCL4*; *CCL3*], Interleukin 1 Beta [*IL1B*]) and M2 markers (*CD163*, Mannose Receptor C-Type 1 [*MRC1*], *CD36*); concurrently, many prototypic marker genes have low expression, i.e., *CD80* and Transglutaminase 2 (*TGM2*) (Figure 3F). Collectively, these findings suggest that HBCs actively shape, sense, and interact with their surroundings, are particularly responsive to lipid-soluble molecules, express high levels of CD36, and likely play a major role in regulating angiogenesis. Next, we were

interested to find out how chromatin-level regulation is supporting this transcriptional and likely functional diversity in HBCs.

HBCs have a distinct chromatin openness profile and have a cell type-specific set of promoters and enhancers

Next, we decided to carry out ATAC-seq experiments to determine the chromatin accessibility in HBC isolates and compare those to published data on human AMs from the lung (19) and MDMs (18), representing a cell type typically responding to inflammatory stimuli. The correlation heatmap shows uniformly high sample–sample similarity among HBC samples, and strong correlations across patients, indicating high data consistency and reproducibility (Supplementary Figure 7A).

As shown in Figure 4A (bottom panel; C7), 27,743 genomic regions show similar chromatin accessibility between HBCs, MDMs, and AMs. However, we were able to detect 25,708 genomic regions, which show significant differences ($p \leq 0.05$; $FC \geq 1.5$) in chromatin accessibility (Figure 4A, top panel). These regions can be grouped into six clusters: three of them are cell type-specific (C1-C3), while the other three are characteristic of two cell types each (C4-C6). To uncover the DNA-binding motifs at these distinctly open genomic regions, we carried out *de novo* motif enrichment analyses separately for the TSS-proximal (promoter) and TSS-distal (enhancer) genomic regions (Figure 4B, C).

TSS-proximal regions of C1 (n=647), which are distinct to HBCs, are enriched in certain motifs such as the motifs of the TPA-Response Element binding motif (TRE; 22,26%), cAMP Response Element binding motif (CRE; 4.93%), E26 transformation-specific (ETS; 15.42%) family motif, as well as CCAAT-boxes (7.79%) (Figure 4B). However, GC-boxes, which are enriched in AM and MDM-specific TSS-proximal regions (C2 and C3), are generally absent in HBCs. Interestingly, the Regulatory Factor X binding motif (RFX) is present at 7.63% of

peaks in HBCs and is enriched in the common regions between HBCs and AMs (C4, 9.12%) (Figure 4B and Supplementary Figure 7B).

The significantly more open TSS-distal regions of all three macrophage subtypes are enriched for myeloid-specific motifs, such as PU.1, TPA-Responsive Element (TRE), cAMP-response element (CRE), or Runt-related transcription factor (RUNX) binding motif. While AM can be characterized by the presence of the already described CEBP (33.81%), Early Growth Response (EGR; 24.03%) motifs, and the motifs of certain bHLH proteins, such as Activating Enhancer-Binding Protein 4 (AP-4; 20.34%), appear to be specific for MDMs. HBCs have shown distinct enrichments for nuclear receptors (NRs) such as NR4A (e.g., NUR77 [13.79%]; Figure 4C and Supplementary Figure 7C), and a sequence motif containing a potential MAF binding site (MARE half site; 10.19%), which only differs from the Forkhead Box (FOX) motif by a single nucleotide (37–39).

Combining the bulk RNA-seq and ATAC-seq data allowed us to associate the enriched motifs with their potential regulator transcription factor(s) using gene expression data. Figure 4D depicts NR4A and RFX target genes that display significantly higher expression (RNA-seq C1) and where NR4A and RFX motifs are located within more accessible chromatin regions in HBCs (ATAC-seq C1). IGV genome browser views of representative NR4A and RFX target genes are presented in Supplementary Figure 8. As shown in Figure 4E, several members of the RFX transcription factor family are expressed in HBCs, such as *RFX1*, *2*, and *RFX5*, of which the latter has the highest expression level. As Figure 3B depicts and Figure 4F further outlines, numerous nuclear receptors show high expression in HBCs, out of which NR4A family members are definitely worth highlighting, given that their binding motif also shows enrichment (Figure 4C). Both Figure 3B and Figure 4F underscore the high expression of *GR*. Furthermore, by using a dataset representing GR target genes, we recognized that the GR is likely to be active due to the high induction levels of many glucocorticoid target genes (Fig

3D) (32). These data, combined with the gene sets presented in Figure 3A, B, and Fig 4F, strongly suggest that HBCs have active metabolic signaling involving nuclear receptors and lipids. Interestingly, by overlapping the HBC-specific opened TSS-proximal (promoter) regions and the HBC-specific genes from C1 of Figure 2D, only a small subset of opened promoters could be associated with HBC-specific gene expression (Figure 5A). We identified 91 promoters, resulting in a 28.12% enrichment of the SREBP-like motif. Based on gene expression data, SREBP1 will most likely bind this motif in HBCs (Figure 5B). Since the enriched motif contains the sequence "TCA", to rule out the possibility that an incomplete or distorted TRE motif was enriched, we mapped the TRE motif and found no significant presence in the 91 promoter regions (Figure 5C). Promoters with a SREBP-like sequence are found in genes such as *SLC25A4*, as well as *PCHD18*, *PCDH12*, *FOXA1*, and *S1PR1* (Figure 5D). These results further underscore the role of HBCs in lipid and fatty acid metabolism; however, this is likely a subset and not a complete set of gene-regulatory region pairs due to the statistical approach.

HBCs exhibit synergistic transcriptional activation upon exposure to IL-4 and rosiglitazone

These findings prompted us to examine the *in vitro* programmability of HBCs using an established signaling paradigm as a proof of concept. Given the fact that CD36 is a key lipid mediator and scavenger receptor with likely functions regarding lipid handling, we decided to test if its expression can be modulated using the well-established model of IL-4-induced and ligand-activated PPARγ (Figure 6.) (40). Therefore, we set up *in vitro* cultures and treated cells with IL-4 and/or rosiglitazone (RSG) (Figure 6A). We present a representative experiment of biological replicates from HBCs isolated from a single placenta (Figure 6B). Treating cells with these ligands results in synergistic gene expression of *CD36*, Angiopoietin Like 4

(*ANGPTL4)*, and Interleukin 1 Receptor Antagonist (*IL1RN)*, providing proof of concept data for the programmability of HBCs. Similar results were obtained from other placentas (Supplementary Figure 9).

Single-Cell CyTOF Profiling Maps Myeloid Phenotypes and Maturation States in HBCs

Finally, we performed CyTOF to complement the gene expression data with qualitative and quantitative single-cell protein expression data and to examine the potential degree of single-cell heterogeneity in our HBC isolates.

Manual gating was used to determine the percentage of HBCs positive for the investigated 14 markers within the living singlets (Figure 7A). The gating strategy is shown in Supplementary Figure 10. In general, HBCs displayed a phenotype similar to immature myeloid cells, characterized by the percentage of $CD45^{+}$ (including low/dim/bright) cells falling between 67-83% (mean: 75.9%, SD: 8.9%). The percentage of HBCs for positive of other myeloid markers are as follows: CD11b, mean: 13.7%, SD: 10.7%; CD11c, mean: 14.5%, SD: 13.2%; CD14, mean: 23.8%, SD: 9.2%; CD16, mean: 8.9%, SD: 8.3%; HLA-DR, mean: 65.5%, SD: 15.7% (Figure 7A). 81.6% (mean, SD: 9.9%) of HBCs showed positivity for the CD36 fatty acid translocase.

The t-distributed stochastic neighbor embedding (t-SNE) analysis deconvoluted the immune landscape of HBCs (Figure 7B). The CD45 and HLA-DR bright and also the CD11b, CD11c, CD14, and CD16 myeloid lineage marker molecules positive hotspots of the visualization of stochastic neighbor embedding (viSNE; demonstrates the distribution of single cells in the mathematical 14-dimensional space [n=14, the number of markers under investigation]) plots represented HBCs with a mature phenotype, however, there are cells showing uncommitted or maybe immature phenotype within the population that was negative (blue spots) for the investigated markers (Figure 7B). The single-cell heterogeneity of the

HBCs was further revealed by the unsupervised FlowSOM (self-organizing maps for visualization and interpretation of cytometry data) analysis of CyTOF data (41). The FlowSOM could generate five metaclusters (MCs) representing differential protein level expression patterns of these functional markers, highlighting the heterogeneity of HBCs.

We identified seven out of fourteen markers differentiating the five FlowSOM MCs of which MC1 ($CD11b^{+}/CD45^{+}/CD11c^{+}/CD14^{low}/CD16^{-}/CD33^{+}/HLA\text{-}DR^{+}$) and MC4 ($CD11b^{low}/CD45^{+}/CD11c^{+}/CD14^{low}/CD16^{-}/CD33^{-}/HLA\text{-}DR^{+}$) represent mature cells, MC3 ($CD11b^{-}/CD45^{low}/CD11c^{-}/CD14^{-}/CD16^{-}/CD33^{-}/HLA\text{-}DR^{-}$) and MC5 ($CD11b^{-}/CD45^{-}/CD11c^{-}/CD14^{-}/CD16^{-}/CD33^{-}/HLA\text{-}DR^{-}$) represent immature cells, and MC2 was a transitional cluster ($CD11b^{-}/CD45^{+}/CD11c^{-}/CD14^{low}/CD16^{-}/CD33^{-}/HLA\text{-}DR^{+}$) (Figure 7C). Regarding the HLA-DR expression patterns, our findings are in line with the findings of Yoshida et al (42).

Thus, based on the CyTOF immunophenotyping, we found that HBCs with relatively low expression of myeloid markers represent a mixture of mature and immature pool of cells. The plasticity of HBCs with the possible transition among the states identified by CyTOF remains a question and needs further study.

DISCUSSION

Fetal-derived tissue-resident macrophages play an essential role in several processes during embryogenesis, including angiogenesis, neurogenesis, bone formation, hematopoiesis, and providing a source of cellular proliferation for tissue-resident macrophages throughout the body (43, 44). Considering the literature and recent findings on HBCs' unique origin, gestational adaptations, and the placenta's significance, this cell type emerges as an intriguing research topic in biology and medicine; however, molecular mechanisms controlling HBCs have yet to be elucidated. The primary aim of this study was to isolate pure human HBCs, free from contamination by maternal or non-macrophage fetal cells, to enable access to a clean, HBC-specific transcriptional profile. We used bulk RNA-seq to assess emerging gene expression patterns, and to maximize sensitivity for low-abundance transcripts, such as transcription factors, which are often underrepresented in single-cell data. Thus, this approach also complemented our bulk ATAC-seq analysis, allowing us to link gene expression with chromatin accessibility and identify candidate regulatory factors with greater confidence. Comparing term HBC transcriptomes to other fetal and adult human macrophages helped to contextualize HBC gene expression patterns and shed light on substantial differences with possible functional significance. The regulation of angiogenesis, placental lipid metabolism and transplacental lipid transport, emerge as key functions of term HBCs. Gene expression data raises the question of whether HBCs have potent antimicrobial properties. Through our *in vitro* induction experiments we could gain insight into the gene expression regulation of CD36. In order to bridge the gap between the bulk nature of our approach, we implemented CyTOF analysis to study cellular heterogeneity on a proteomic level and identified myeloid phenotypes and heterogenous maturation states in our isolates. This approach provides foundation for basic

biology, disease modeling, and translational applications by identifying distinct gene expression pattern (including DEGs, and HBC specific transcripts).

The likely functions of HBCs based on gene expression

Based on our results and analysis, the HBCs have a distinct gene expression pattern different from other fetal and adult macrophage subpopulations. Assessing the function of highly or exclusively expressed individual genes and emerging gene expression patterns we found that are HBCs play a role in maintaining placental structural and functional integrity (high ranking of ECM genes on Figure 3A; Supplementary Figure 5B), development of placental microarchitecture (high ranking of Angiogenesis genes on Figure 3A; Supplementary Fig 5A), lipid metabolism and lipid signaling (high ranking of nuclear receptor genes on Figure 3A and Fig, 3B). The low ranking of Microorganisms genes suggest that third trimester HBC have inferior antimicrobial properties within this comparative context (Figure 3A and Supplementary Figure 6C). This finding resonates with the findings of Yoshida et al., who found that term HBCs have diminished activity against *L. monocytogenes* infection compared to first trimester HBCs (42).

Dissecting the list of DEGs highly expressed in HBCs can serve as a basis for subsequent experiments characterizing cell type functions using mechanistic approaches. High expression of *SEPP1* suggests HBCs' role in maintaining placental oxidative balance and transplacental selenium transport, while *TGFB1* emerges as a cytokine with substantial role in HBC-TB communication or maintaining immunological balance at the fetal-maternal interface. Furthermore, many complement components and regulatory factors, including *C1QA, C1QC*, and *VSIG4* are exceptionally highly expressed genes located in cluster C1. Previous literature suggest the significance of placental complement cascade dysregulation in the pathophysiology of villitis of unknown etiology (VUE) (45, 46), and in the pathogenesis of preeclampsia (47).

Supporting the relevance of this pathway, studies have shown that C1 complex-deficient mice exhibit reduced litter sizes, and that anti-C1q antibodies may contribute to recurrent pregnancy loss in individuals with lupus nephritis and antiphospholipid syndrome (48, 49). The enrichment of complement components term HBCs were also highlighted by Yoshida et al. (42).

Identification of specific and selective HBC genes

Gene expression data alone is rarely sufficient to draw definitive conclusions about a gene's function. However, comparing the expression of specific genes across different cell types can generate stronger, testable hypotheses about the roles of those cell types (Figure 2E). Within this comparative context, we identified several HBC-specific genes known to play a role in gestational physiology and are associated with various diseases, including pregnancy complications. Examples include *TAC3* associated with infertility a (50), *CSH1* with choriocarcinoma (51), and *PAPPA2* with pre-eclampsia (52).

H19 and *IGF2* form an imprinted cluster on chromosome 11 whose lncRNA and growth factor products reciprocally regulate fetal and placental development (53, 54). *H19* is expressed from the maternal allele and limits growth, in part by repressing *IGF2*, which when expressed from the paternal allele promotes placental nutrient transport, hormone secretion and trophoblast differentiation/invasion. Their activity is modulated by IGF-binding proteins, notably *IGFBP3* and *IGFBP4* (cluster 1 HBC–specific genes), and misregulation underlies Silver-Russell and Beckwith-Wiedemann syndromes both of which are growth disorders (55–57). NOTUM, a secreted WNT deacetylase, restrains WNT-driven trophoblast stem cell maintenance to permit extravillous differentiation, while APOLD1 organizes endothelial junctions and cytoskeletal architecture to regulate barrier permeability (58, 59).

The epigenomic underpinning of HBC gene expression

Comparing ATAC-seq data from HBCs with ATAC-seq data from healthy human AMs and MDMs revealed insights into HBC gene expression regulation. Regarding promoter regions, we hypothesize that enrichment of the RFX binding motif and gene expression of RFX family member genes may indicate a transcription factor with a potential role specific to either the cell type or the gestational phase in HBCs. RFX factors, that share a common DNA-binding motif are indispensable for MHC II expression; mutations in RFX genes cause Bare Lymphocyte Syndrome, leading to drastically reduced MHC II expression on immune cells (60, 61). The high expression of RFX5 and the enrichment of its binding motif aligns with previous findings on the transition between first-trimester HLA-DRneg HBCs and third-trimester HLA-DRpos HBCs, as well as with our CyTOF analysis (Figure 7) (42). Further dissection of the RFX transcription factor family's functional relevance requires a mechanistic approach, possibly involving animal studies, epigenetic analysis, or gene knock-down experiments.

The enrichment of transcription factor binding motifs characteristic of myeloid cells, as well as motifs binding NR4A members and estrogen receptors in the HBC-specific enhancer cluster resonate with gene expression data that highlighted the significance of nuclear receptor signaling (Figure 3A) with high expression of certain nuclear receptors, and GR regulated genes. If FoxA1 is capable of binding to the motif, it may also serve as a pioneer transcription factor for Estrogen Receptor Alpha (ERα), which could bind the IR3 NR motif (enriched by 7.07%) within HBCs (Figure 4C). These findings lay foundation for future projects focusing on cell identity and differentiation, more extensive mechanistic experiments to study HBC responsiveness and to find potential therapeutic targets.

HBCs as lipid-rich and lipid-handling macrophages

Cellular morphology, enrichment of nuclear receptor binding sites and high expression of certain nuclear receptors, *CD36*, *PLTP*, *SREBP1*, ATP Binding Cassette Subfamily A Member 1 (*ABCA1*), and ATP Binding Cassette Subfamily G Member 1 (*ABCG1*), all converge in the same direction, highlighting fatty acid and cholesterol functionality in HBCs (Figure 2D). CD36, a key scavenger and lipid uptake receptor under the control of PPARγ, CEBPα and Nuclear Receptor Subfamily 1 Group D Member 2 (NR1D2) has several ligands including free fatty acids, lipoproteins (e.g., LDL), collagen, and thrombospondin (62, 63). CD36 is present in several tissues and cell types but has an unclear role and a vague pathological significance in the placenta. Dubé et al. found an association between maternal obesity and increased newborn cholesterol and LDL levels, as well as increased placental *CD36* expression at both mRNA and protein levels (64). CD36 is crucial in forming foamy macrophages in atherosclerotic lesions, morphologically similar to HBCs on microscopic Cytospin images. While CD36 is well-characterized as a scavenger receptor in other macrophage populations, its specific function in HBCs remains undefined. Its expression suggests a potential role in lipid uptake and clearance of cellular debris or microbial antigens, but direct functional evidence in the placental context is currently lacking. Performing CyTOF analysis allowed us to examine CD36 expression in the HBC isolates on the protein level. The consistently high expression of CD36 protein in all subgroups (Figure 7A-C) backs the gene expression data and supports the proposed significance. Notably, our clinical inclusion/exclusion criteria may not exclude the influence of maternal metabolic imbalances on placental microenvironment, as we didn't consider maternal obesity or laboratory parameters indicative of metabolic status. However, as part of physiologic changes in pregnancy, maternal blood levels show a natural increase (65). In this context, the significant increase in leptin mRNA expression in pre-eclamptic placentas contributes to altered immune and metabolic functions and may support the existence of a pathway by which HBCs may be linked to the pathogenesis of this pregnancy complication of

high morbidity (66). Whether this is a correlative or causative relationship remains to be determined.

Our IL-4 and RSG-mediated PPARγ induction experiments, although limited in its scope, confirmed the interaction of the pathways and raised the possibility of synergistic interactions (e.g., *CD36*, *ANGPL4*, *IL1RN*), which need to be verified using dose-response studies (Figure 6B). These experiments further underpin the adaptability of HBCs and pave the way for testing additional ligands to alter gene expression, intercellular interactions, and ultimately the function or pathophysiological role of HBCs.

All HBC isolates analyzed in this study were derived from healthy, term placentas delivered via cesarean section. While our data establish a foundational "parts list" of gene expression in normal HBCs, future studies are needed to investigate how gene expression and regulatory programs may vary with pregnancy complications or gestational age. Our findings support the hypothesis that HBCs possess distinct transcriptional and regulatory profiles; however, they also raise new questions that extend beyond the scope of this work.

An important area for future investigation is the interaction between HBCs and neighboring cells, including trophoblasts, endothelial, and mesenchymal cells. Given species-specific differences in placental structure and physiology, addressing this question may require advanced models such as organoids, co-cultures, microphysiological systems, *in vivo* imaging, and *in silico* tools like CellChat. Furthermore, given the specificities of each trimester during pregnancy, the function of HBCs may show dynamic changes and adaptations at different times and, remarkably, ready programmability even at term (67).

This exploratory study provides a foundational multi-omic characterization of term HBCs. We acknowledge that a limitation of this study is the relatively small sample size (n=5 donors), which could lower our power to capture biological variation in this system. Nonetheless, donor-to-donor correlation was high as observed in our gene expression (Pearson's correlation ≥ 0.77)

and chromatin accessibility assays (Pearson's correlation ≥ 0.88), indicating that our donors showed high overall transcriptomic and epigenomic similarity. In spite of the homogeneity among the donors, we showed that consistent molecular features differentiate HBCs from other fetal and adult macrophage populations, irrespective of the assay used (CyTOF: 5 donors; qPCR/RNAseq 4 donors; ATACseq 3 donors). Importantly, this level of correlation is also consistent with intra-population variation estimates from cellular atlases such as the Tabula Sapiens, where gene expression among resident macrophages in the same tissue was highly correlated (68). It should be noted that acquiring human placental samples for research is a challenging task (given the ethical concerns, strict inclusion and exclusion criteria, etc.), and this study represents an important step towards the exploration of this unique and specialized immune cell population. As with any study using human samples, future studies are always warranted to include larger cohorts to capture additional variation. While we identified transcriptional and chromatin programs suggesting regulatory roles for nuclear receptors such as PPARγ and NR4A family members, functional validation of these pathways *in vivo* remains to be done. Finally, although *in vitro* stimulation assays indicated transcriptional plasticity, we did not perform additional functional assays, such as lipid uptake, phagocytic or co-culture experiments in this study, these assays can be included in future studies. Ongoing work to develop *in vitro* placental models and functional assays will be essential to validate and expand upon these findings.

Overall, these results will lay the foundation for further studies focusing on the isolation and characterization of HBCs from placentas from complicated pregnancies, applying single-cell approaches to uncover the degree and characteristics of heterogeneity, and *in vitro* analyses of programmability and cell-cell interactions (i.e., TBs, endothelial cells) using co-cultures and microrheological systems

METHODS

Participants involved in the study

Participant selection was based on inclusion and exclusion criteria as shown in Supplementary Table 2. An overview of donor samples and associated technical replicates used across the experiments and analyses is provided in Supplementary Table 3.

Tissue processing and cell isolation

To gain HBCs of an appropriate number and purity, we adapted the protocol of Tang et al. (68). Briefly, the placentas were transferred to a BSL-2 laboratory within 20 minutes of delivery. The fetal membranes were first separated, and the villous tissue was obtained by dissecting the placenta. The tissue was minced and rinsed with calcium- and magnesium-free phosphate-buffered saline (PBS). The chopped tissue was digested in 3 cycles with 0.25% trypsin (ThermoFisher Scientific)/0.08mg/mL DNase I (Roche) digestion solution (37°C water bath with orbital shaker for 15, 30, 45 minutes, respectively). The undigested tissue fragments (containing HBCs) were digested in 1mg/ml Collagenase A (Roche)/ 0.1mg/ml DNase I digestion solution (37°C water bath with orbital shaker for 45 minutes) followed by filtration through a 100 μm sieve. The pooled and filtered cell suspensions were centrifuged before separation of HBCs by Percoll (GE) gradients. 7.5 mL of 40%, 35%, 30%, and 20% Percoll gradients were used, and 5 mL of cell suspension was layered on top of the gradients. The suspension-loaded gradients were centrifuged for 20 minutes at 1,200g, at room temperature (RT), without brake. The HBCs were found at the interface between 35% and 30% to interface between 30% and 20%. After gradient-based cell separation, the cell suspension was further purified by incubating with magnetic beads (Invitrogen) conjugated to anti-EGFR (sc-120, Santa Cruz Biotechnology) and anti-CD10 (#312202, BioLegend) antibodies, using 25 μL of

beads per 10 million cells. The cell suspension was collected, and the beads were removed by placing the suspension into a paramagnetic field. The total cell number was then counted.

Flow cytometry analysis and cell sorting

The $EGFR^-$ $CD10^-$ cells were labeled for anti-hCD163-APC (#333609, Biolegend) antibody. The FcR Blocking Reagent (Miltenyi Biotec) was used to prevent the non-specific binding of antibody conjugates. To discriminate live and dead cells, the eBioscience™ Fixable Viability Dye eFluor™ 506 (Thermo Fischer Scientific) was used based on the manufacturer's recommendation. The $CD163^+$ HBCs were sorted by FACSAria™ III (BD Biosciences) based on cell size, singularity, viability, and CD163 positivity, and HBCs were used for cytospin, RNA-seq, and ATAC-seq analysis.

Quality control of the applied HBC isolation process using single-cell RNA sequencing

Initially, quality control filtering was applied to the single-cell data, aiming to retain only viable cells. Cells falling within the extreme 0.5th percentile of both the number of identified features and total count distributions were excluded. Additionally, cells in which mitochondrial counts constituted more than 15% of the total counts were filtered out (Supplementary Figure 2A, B). The quality control approach maintained the nFeature/nCounts ratio at 0.9, indicating a strong correlation between these two features and suggesting a minimal presence of doublets.

The single-cell analysis allowed us to perform unsupervised cell type annotation through the SingleR package. By comparing our cells' transcriptional profile to those from the Human Primary Cell Atlas database (64), the software identified two major cell identities (Supplementary Figure 2C). The largest population, comprising 89.2% of total cells, had a clear macrophage/monocytic identity, being automatically annotated as such. The second, 9.8% of the cells, had a mixed profile ranging from "Tissue Stem Cells" to "Fibroblasts".

Determination of maternal contamination

To assess potential maternal cellular contamination, we developed a protocol predicting contaminating non-fetal cell proportions based on sex-associated gene expression differences. Using a Single-Cell Transcriptomics library from a female/female sample, we derived a pseudo-bulk RNA to estimate XIST expression (69). Comparing XIST expression percentages in male offsprings' bulk RNA female/male to female/male samples (Percentage in female/male sample / Percentage in female/female sample * 100) reveals insights into maternal contamination, given the child's gender. To further complement quality control, we performed principal component analysis (PCA) comparing HB cells to two subpopulations of decidual macrophages (dM1, dM2), maternal placental macrophages (PM3), first-trimester Hofbauer cells (HBP_FT) and third trimester Hofbauer cells (HBP_TT). Reference single-cell RNA-seq data (dM1, dM2, PM3, HBP_FT) were obtained from the publication of Vento-Tormo et al (13) and HBP_TT from Sureshchandra et al (16). Following standard quality control (doublet removal, feature/count thresholds), cells were subset based on original annotations and stratified by biological replicate. Samples with fewer than 100 cells per cell type and biological replicate were excluded. Remaining cells per replicate were aggregated into pseudobulk profiles.

To integrate pseudobulk data with our bulk RNA-seq HB dataset, both were normalized for library size and merged by intersecting gene sets. Batch effects between pseudobulk and bulk data were corrected using SVA prior to PCA.

Collection of public RNA- and ATAC-seq data

Publicly available fetal and adult RNA-seq and adult ATAC-seq data were collected from the Sequence Read Archive (SRA) database, and the raw sequences were downloaded from the

European Nucleotide Archive (ENA) database of the EMBL-EBI. The list of the used data and their identifiers is available as a (Supplementary Table 4).The raw values are provided in a supplementary dataset (Supplementary Table 5 and Supplementary Table 6).

RNA-seq analysis

RNA-seq analysis was carried on out n=4 placentas. Out of three placentas, two technical replicates were involved to assess variability, technical consistency, and strengthen quality control.

Raw sequence reads of all RNA-seq data were uniformly aligned to the hg19 reference genome assembly with HISAT2 (v2.1.0) using default parameters (70). From the BAM files, transcripts were assembled with StringTie (v1.3.4d) (71). BAM files were indexed with SAMtools (v1.7), and then coverage (bedgraph) files were generated by HOMER's makeUCSCfile program (72, 73). Gene expression levels were determined in FPKM (Fragments Per Kilobase of transcript per Million mapped reads) values.

For secondary analyses, genes that showed a higher than 0 FPKM value in at least one sample were considered expressed and included in the comparative analyses. Then, for each sample, the FPKM value was normalized by the decile value of the given sample. The differentially expressed genes were determined with one-way ANOVA supplemented with a post-hoc Tukey HSD statistical test using the stats, tidyverse, and sqldf packages in R. The applied cut-off values (0.05 as p-value and 2 as fold difference (FD)) were indicated in the figure descriptions in all cases. The multidimensional scaling (MDS) plot was generated by plotMDS function of the limma package, the sample-to-sample distance plot was visualized by the edgeR and pheatmap packages, and the Pearson correlation-based heatmap was generated using the pheatmap package in R (v3.5.1) (74). Only bulk RNA-seq datasets were compared to our own bulk RNA-seq result and were included in the (Figure 2, Figure 3, Figure 4, Figure 5,

Supplementary Figure 4, Supplementary Figure 5, and Supplementary Figure 6). The biological pathways were predicted with Metascape (v3.5.20230501) (75). K-means clustering of the genes was carried out by Cluster 3.0, and the applied similarity metric was the centered correlation (76).

Genes for the sensing repertoire of tissue-resident macrophages were collected from the original article and were supplemented with the members of the gene or receptor (super)families and lectins (30, 77). Genes, with an average normalized expression lower than 0.5 FPKM in all tissue types, were not shown. Gene sets for the functional analysis were derived from the Panther database. Normalized expression values for the consensus gene set, the genes associated with the clusters, and those encoding macrophage-specific TFs are listed in Supporting Data.

In vitro induction

Primary HBCs (from n=4 placentas) after isolation and sorting were plated onto multiwell culture plates (approximately 1 million cells per well) in RPMI supplemented with 5% fetal bovine serum, 1% penicillin/streptomycin and 25mM HEPES. We treated freshly plated HBCs with IL-4 (20 ng/μL) and/or synthetic agonist of PPARγ, RSG (1 μM). Cells were harvested 24 hours after cytokine and ligand treatment. Co-treatment happened simultaneously. Total RNA was isolated from cells using Tri Reagent (MRC) according to manufacturer's protocol. RNA was transcribed into cDNA; transcript quantification was performed by quantitative real-time polymerase chain reaction (RT-PCR) using user designed Taqman assays or Taqman Gene Expression Assays. Gene expression was quantified by the comparative threshold cycle method and normalized to cyclophilin A expression (Czimmerer et al, 2012). The raw values are provided in a supplementary dataset (Supplementary Table 7).

ATAC-seq analysis

ATAC-seq analysis was carried out on n=3 placentas. Out of 2 placentas, two technical replicates were involved to assess variability, technical consistency, and strengthen quality control.

Raw sequence reads were aligned to the hg19 reference genome assembly with default parameters by using the BWA tool (v07.17); single-end reads were aligned by setting the *samse*, paired-end reads were aligned by using the *sampe* parameter (78). BAM files were generated with SAMtools (v1.7) (70). Narrow peaks were predicted with the callpeak function of MACS2, and their widths were fixed to 200 bp relative to their summits (79). Artifacts were removed according to the blacklisted genomic regions of ENCODE (80). Genome coverage (bedgraph) files were generated by HOMER's makeUCSCfile, then they were indexed to tdf files with igvtools (v2.3.98) (81). The fragment length was set to 150 bp.

For the secondary analyses, a consensus peak set was generated by using the mergeBed command of bedtools (v2.27.1) (82). Peaks that could be predicted from at least 5 samples were part of the consensus set. Then, for each sample, Reads Per Kilobase per Million mapped reads (RPKM) values were calculated on the consensus peak set by the coverageBed command of bedtools, and the RPKM values were normalized by the decile value of the given sample. The Pearson correlation-based heatmap was generated using the pheatmap package in R (v3.5.1)

By using the decile normalized values, the differentially accessible chromatin regions were defined by one-way ANOVA supplemented with a post-hoc Tukey HSD statistical test. As cut-off, $p \leq 0.05$ and $FD \geq 2$ were applied. K-means clustering of the genomic regions was carried out by Cluster 3.0, and the applied similarity metric was the centered correlation (76).

The consensus peak set, the differentially accessible chromatin regions, and the regions associated with the clusters are listed with their normalized RPKM values in Supporting Data.

De novo motif enrichment analysis

First, the separation of the TSS-proximal (promoter-TSS and 5' UTR) and TSS-distal (introns, intergenic, exons, 3' UTR, and TTS) regions was determined by HOMER's annotatePeaks. Then, *de novo* motif enrichment analysis was carried out by HOMER's findMotifsGenome.pl program and was performed on the summit+/-100 bp regions of all the TSS-proximal (promoter) and the summit+/-100 bp of the top 1,000 TSS-distal (enhancer) regions (72). The targeted motif lengths were 10, 12, 14, and 16 bp. P-values were calculated by comparing the enrichment within the target regions with that of a random set of regions (background) generated by HOMER.

Visualization

Row-normalized gene expression heat maps were visualized in R by the pheatmap package. Heat maps representing absolute gene expression values were visualized by JavaTreeView v1.1.6r4 (83). Bar charts and dot plots were plotted by using GraphPad Prism v.9. Genome coverage (bedgraph) files were visualized by IGV v2.4.16, where the replicates that belong together were depicted as overlay tracks (81). Figure 6A was created in https://BioRender.com

Mass Cytometry

All 5 placentas were involved for mass cytometry analysis.

Single-cell mass cytometry was performed as described previously by our group with minor modifications (84, 85). Briefly, cryotubes were thawed in a 37°C water bath for 2 min,

and cells were transferred into 14 ml RPMI (Capricorn) at 37 °C and centrifuged at 350 g for 6 min (washed) at room temperature (24 °C, RT). Cells were washed once more with 10 ml RPMI, cells were counted using a Bürker-chamber, and viability was determined by Trypan Blue (Merck) exclusion. Cells were washed with 2 ml Maxpar Cell Staining Buffer (MCSB, Fluidigm), resuspended in 500 µl MCSB-containing Cell ID™ ^{195}Pt-cisplatin (Standard BioTools) (stock 5 mM, 1,000X diluted), and incubated for 3 min on ice. Cells were washed with 2 ml MCSB two times and resuspended in 50 µl MCSB supplemented with 1:20 v/v TruStain FcX™ FC receptor blocking solution (Biolegend) and incubated at RT for 10 min. Cells were stained with the Human Monocyte-Macrophage Phenotyping Panel Kit (Standard BioTools) according to the instructions of the manufacturer in the final volume of 100 µl MCSB and incubated at RT for 30 min. The antibodies used for CyTOF are listed in the Supplementary Table 8. Cells were washed twice with MCSB, prefixed with 500 µl of Pierce™ formaldehyde (stock w/v 16%) (Thermo Fisher Scientific) solution diluted in PBS to 1.6%, and incubated at RT for 10 min. Stained and prefixed cells were centrifuged at 800 g at RT for 6 min and resuspended in 800 µl Fix & Perm solution (Standard BioTools) supplemented with 1:1,000 [v/v] ^{191}Ir-^{193}Ir DNA intercalator (Standard BioTools) for overnight incubation. Samples were washed two times with MCSB, and once with PBS, filtered through a 30 µm Celltrics gravity filter (Sysmex). The cell concentration was adjusted to $7x10^5$/ml in Cell Acquisition Solution (CAS, Standard BioTools) including EQ four-element calibration beads (Standard BioTools) at a 1:10 ratio [v/v]. Applying the WB injector (Standard BioTools), cells were acquired using a properly tuned Helios mass cytometer (Standard BioTools). The generated flow cytometry standard (FCS) files were randomized and normalized with the default settings of the internal FCS-processing unit of the CyTOF Software (Fluidigm, version:7.0.8493). The randomized and normalized FCS files were uploaded to the Cytobank analysis platform (Beckman Coulter).

Link: https://premium.cytobank.org/cytobank/experiments/494993

Exclusion of normalized beads, dead cells, debris, doublets, and manual gating was performed as presented in Supplementary Figure 10. The percentage of the populations defined by manual gating was plotted in GraphPad Prism 8 (Dotmatics). The anti-CD7 signal with close intensity to the background was excluded from subsequent analysis. In total, 300,000 single-cells and 14 markers were used to create a t-SNE map of Hofbauer cells. High-dimensional reduction and visualization were performed using the (t-SNE) algorithm. For the unsupervised definition of main subpopulations, we performed a self-organizing map-based FlowSOM metaclustering analysis. The CyTOF marker intensities were inverse-hyperbolic sine-transformed (arcsinh) with cofactor 5 in Cytobank. We identified 5 different metaclusters that were separately subclustered in another round of FlowSOM.

The FlowSOM was performed in Cytobank Premium. The expression intensities were expressed as arcsinh values that were calculated by applying the arcsinh equation divided by the scale argument to the measured metal intensity value. The marker expression intensities of the acquired HBCs in CyTOF were beyond the values of peripheral myeloid cells using the commercially available Human Monocyte-Macrophage Phenotyping Panel Kit for CyTOF. Reference PBMC samples were acquired simultaneously with the HBCs as an internal control (data not shown).

Sex as a biological variable

The study involved 3 male and 2 female newborns.

Statistics

For RNA-seq analysis, differentially expressed genes were identified by one-way ANOVA with post-hoc Tukey HSD (using the stats, tidyverse, and sqldf packages in R). Genes with

$P \leq 0.05$ and a fold difference (FD) ≥ 2 were considered significant. Scatter plots indicate mean (line) and ± SD (whiskers).

For ATAC-seq analysis, differentially accessible chromatin regions were defined by one-way ANOVA with post-hoc Tukey HSD, applying the same thresholds ($P \leq 0.05$ and $FD \geq 2$). K-means clustering of genomic regions used centered correlation as the similarity metric. *De novo* motif enrichment was assessed in HOMER by comparing the target regions to a random set of regions (background), with significance determined by $P \leq 0.05$.

Study approval

All the procedures were approved by the Ethics Committee of the University of Debrecen (protocol number: DE RKEB/IKEB 6426-2023) and the Policy Administration Services of Public Health of the Government Office (protocol number: BM/1425-3/2024). Informed written consent was obtained from all the participants involved in this research, and the study was performed in agreement with the ethical standards of the Declaration of Helsinki.

Data availability

The generated next-generation sequencing data sets are available in the Gene Expression Omnibus (GEO) repository under GSE255954 (ATAC-seq) and GSE255955 (RNA-seq).

ACKNOWLEDGEMENT

We would like to express our gratitude to Dr. Szilard Poliska for conducting the RNA-seqs and ATAC-seqs, Mr. Jordan Scherer for his insightful comments and meticulous proofreading of the manuscript, and the physicians and staff of the Department of Obstetrics and Gynecology, Faculty of Medicine, University of Debrecen for their invaluable assistance in acquiring the placentas and members of the Nagy laboratory for discussions and comments on the manuscript. We are grateful to Dr. Oscar Ospina for his valuable assistance and guidance with bioinformatics and biostatistics.

FUNDING

BRB is supported by the EKÖP-25-3 university research scholarship program of the Ministry of Culture and Innovation from the source of the National Research, Development and Innovation Fund. This work was partially supported by the National Research, Development, and Innovation Office (NKFI), Hungary (OTKA K147147, ADVANCED-152422 to the Nuclear Receptor Research Lab and FK142877 to GJS, FK146945 to GN, PD137902 to DB), and by the János Bolyai Research Scholarship of the Hungarian Academy of Sciences (BO/00582/22/8 to GJS). NCS is supported by the European Union's Horizon 2020 research and innovation programme under the Marie Skłodowska-Curie grant agreement No. 860034.

Author contributions

BRB., T.D, and L.N. planned the experimental project, D.B planned the bioinformatic approaches and they drafted the manuscript. B.R.B., K.B., and T.C.S. isolated HBCs from placentas and produced the RNA-seq samples. P.T. carried out the ATAC-seq experiments. D.B., G.N., and J.C.R.F. performed the computational analyses. K.B. and N.C-S. performed the flow cytometry measurements. Patient recruitment was done by T.D. and Z.T.K. M.T.

carried out Cytospin slide preparation. CyTOF was performed and analyzed by P.N. and G.J.S. RT-Q-PCR was executed by B.R.B., K.B., and T.C.S. The HBC isolation protocol was created and adapted with the help of Z.T. and S.G. B.R.B., D.B., G.J.S., J.C.R.F., K.B. and P.N. designed the figures. L.N. directed and supervised the work. All authors discussed the results and commented on the manuscript.

The order of first-authorship was determined by weighing relative contributions to experimental design, execution, analyses, conceptualization, and writing of the manuscript.

REFERENCES

1. Mass E, et al. Tissue-specific macrophages: how they develop and choreograph tissue biology. *Nat Rev Immunol*. 2023;23(9):563–579.

2. Gomez Perdiguero E, et al. Tissue-resident macrophages originate from yolk-sac-derived erythro-myeloid progenitors. *Nature*. 2015;518(7540):547–551.

3. Georgiades P, Ferguson-Smith AC, Burton GJ. Comparative Developmental Anatomy of the Murine and Human Definitive Placentae. *Placenta*. 2002;23(1):3–19.

4. Castellucci M, Kaufmann P. Basic Structure of the Villous Trees. *Pathology of the Human Placenta*. Springer New York; 2006:50–120.

5. Anteby EY, et al. Human Placental Hofbauer Cells Express Sprouty Proteins: a Possible Modulating Mechanism of Villous Branching. *Placenta*. 2005;26(6):476–483.

6. Seval Y, Korgun ET, Demir R. Hofbauer Cells in Early Human Placenta: Possible Implications in Vasculogenesis and Angiogenesis. *Placenta*. 2007;28(8–9):841–845.

7. Tang Z, et al. Placental Hofbauer cells and complications of pregnancy. *Annals of the New York Academy of Sciences*. 2011;1221(1):103–108.

8. Reyes L, Golos TG. Hofbauer Cells: Their Role in Healthy and Complicated Pregnancy. *Front Immunol*. 2018;9:2628.

9. Thomas JR, et al. Primitive haematopoiesis in the human placenta gives rise to macrophages with epigenetically silenced HLA-DR. *Nat Commun*. 2023;14(1):1764.

10. Zulu MZ, et al. The Elusive Role of Placental Macrophages: The Hofbauer Cell. *J Innate Immun*. 2019;11(6):447–456.

11. Kim J-S, et al. Involvement of Hofbauer cells and maternal T cells in villitis of unknown etiology. *Histopathology*. 2008;52(4):457–464.

12. Liu Y, et al. Single-cell RNA-seq reveals the diversity of trophoblast subtypes and patterns of differentiation in the human placenta. *Cell Res*. 2018;28(8):819–832.

13. Vento-Tormo R, et al. Single-cell reconstruction of the early maternal–fetal interface in humans. *Nature*. 2018;563(7731):347–353.

14. Suryawanshi H, et al. A single-cell survey of the human first-trimester placenta and decidua. *Sci Adv*. 2018;4(10):eaau4788.

15. Batorsky R, et al. Hofbauer cells and fetal brain microglia share transcriptional profiles and responses to maternal diet-induced obesity. *Cell Reports*. 2024;43(6):114326.

16. Sureshchandra S, et al. Multimodal profiling of term human decidua demonstrates immune adaptations with pregravid obesity. *Cell Rep*. 2023;42(7):112769.

17. Dong T, et al. Activation of GPR3-β-arrestin2-PKM2 pathway in Kupffer cells stimulates glycolysis and inhibits obesity and liver pathogenesis. *Nat Commun*. 2024;15(1):807.

18. Zhang P, et al. Epigenomic analysis reveals a dynamic and context-specific macrophage enhancer landscape associated with innate immune activation and tolerance. *Genome Biol*. 2022;23(1):136.

19. Correa-Macedo W, et al. Alveolar macrophages from persons living with HIV show impaired epigenetic response to Mycobacterium tuberculosis. *Journal of Clinical Investigation*. 2021;131(22):e148013.

20. Abud EM, et al. iPSC-Derived Human Microglia-like Cells to Study Neurological Diseases. *Neuron*. 2017;94(2):278-293.e9.

21. Douvaras P, et al. Directed Differentiation of Human Pluripotent Stem Cells to Microglia. *Stem Cell Reports*. 2017;8(6):1516–1524.

22. Ahmadzadeh K, et al. Multinucleation resets human macrophages for specialized functions at the expense of their identity. *EMBO Reports*. 2023;24(3):e56310.

23. Fujii T, et al. MEF2C regulates osteoclastogenesis and pathologic bone resorption via c-FOS. *Bone Res*. 2021;9(1):4.

24. Klei TRL, et al. Hemolysis in the spleen drives erythrocyte turnover. *Blood*. 2020;blood.2020005351.

25. Dharmasiri S, et al. Human Intestinal Macrophages Are Involved in the Pathology of Both Ulcerative Colitis and Crohn Disease. *Inflammatory Bowel Diseases*. 2021;27(10):1641–1652.

26. Rhodes JW, et al. Human anogenital monocyte-derived dendritic cells and langerin+cDC2 are major HIV target cells. *Nat Commun*. 2021;12(1):2147.

27. Lissner MM, et al. Age-Related Gene Expression Differences in Monocytes from Human Neonates, Young Adults, and Older Adults. *PLoS ONE*. 2015;10(7):e0132061.

28. Nagy G, et al. Lineage-determining transcription factor-driven promoters regulate cell type-specific macrophage gene expression. *Nucleic Acids Research*. 2024;52(8):4234–4256.

29. Thomas JR, et al. Phenotypic and functional characterization of first-trimester human placental macrophages, Hofbauer cells. *J Exp Med*. 2020;218(1):e20200891.

30. Lazarov T, et al. Physiology and diseases of tissue-resident macrophages. *Nature*. 2023;618(7966):698–707.

31. Tang Z, et al. Glucocorticoids Enhance CD163 Expression in Placental Hofbauer Cells. *Endocrinology*. 2013;154(1):471–482.

32. Reddy TE, et al. Genomic determination of the glucocorticoid response reveals unexpected mechanisms of gene regulation. *Genome Res*. 2009;19(12):2163–2171.

33. Duluc D, et al. Tumor-associated leukemia inhibitory factor and IL-6 skew monocyte differentiation into tumor-associated macrophage-like cells. *Blood*. 2007;110(13):4319–4330.

34. Sica A, Mantovani A. Macrophage plasticity and polarization: in vivo veritas. *J Clin Invest*. 2012;122(3):787–795.

35. Martinez FO, Gordon S. The M1 and M2 paradigm of macrophage activation: time for reassessment. *F1000Prime Rep*. 2014;6. https://doi.org/10.12703/P6-13.

36. Rőszer T. Understanding the Mysterious M2 Macrophage through Activation Markers and Effector Mechanisms. *Mediators of Inflammation*. 2015;2015(1):816460.

37. Cain DW, et al. Identification of a Tissue-Specific, C/EBPβ-Dependent Pathway of Differentiation for Murine Peritoneal Macrophages. *The Journal of Immunology*. 2013;191(9):4665–4675.

38. McCowan J, et al. The transcription factor EGR2 is indispensable for tissue-specific imprinting of alveolar macrophages in health and tissue repair. *Sci Immunol*. 2021;6(65):eabj2132.

39. Swinstead EE, et al. Steroid Receptors Reprogram FoxA1 Occupancy through Dynamic Chromatin Transitions. *Cell*. 2016;165(3):593–605.

40. Szanto A, et al. STAT6 Transcription Factor Is a Facilitator of the Nuclear Receptor PPARγ-Regulated Gene Expression in Macrophages and Dendritic Cells. *Immunity*. 2010;33(5):699–712.

41. Van Gassen S, et al. FlowSOM: Using self-organizing maps for visualization and interpretation of cytometry data. *Cytometry Pt A*. 2015;87(7):636–645.

42. Yoshida N, et al. Interactions between placental Hofbauer cells and *L. monocytogenes* change throughout gestation. *Sci Immunol*. 2025;10(109):eadq3066.

43. Wu Y, Hirschi KK. Tissue-Resident Macrophage Development and Function. *Front Cell Dev Biol*. 2021;8:617879.

44. Lee CZW, Ginhoux F. Biology of resident tissue macrophages. *Development*. 2022;149(8):dev200270.

45. A Lee K, et al. Distinct patterns of C4d immunoreactivity in placentas with villitis of unknown etiology, cytomegaloviral placentitis, and infarct. *Placenta*. 2013;34(5):432–435.

46. Cornish EF, McDonnell T, Williams DJ. Chronic Inflammatory Placental Disorders Associated With Recurrent Adverse Pregnancy Outcome. *Front Immunol*. 2022;13:825075.

47. Agostinis C, et al. A non-redundant role of complement protein C1q in normal and adverse pregnancy. *Explor Immunol*. 2022;622–636.

48. Ohmura K, et al. Pathogenic roles of anti-C1q antibodies in recurrent pregnancy loss. *Clinical Immunology*. 2019;203:37–44.

49. Girardi G, et al. Essential Role of Complement in Pregnancy: From Implantation to Parturition and Beyond. *Front Immunol*. 2020;11:1681.

50. Yang JJ, et al. Uncovering Novel Reproductive Defects in Neurokinin B Receptor Null Mice: Closing the Gap Between Mice and Men. *Endocrinology*. 2012;153(3):1498–1508.

51. Nickel BE, et al. Differential expression of human placental growth hormone variant and chorionic somatomammotropin genes in choriocarcinoma cells treated with methotrexate. *Molecular and Cellular Endocrinology*. 1993;91(1–2):159–166.

52. Crosley EJ, et al. First-Trimester Levels of Pregnancy-Associated Plasma Protein A2 (PAPP-A2) in the Maternal Circulation Are Elevated in Pregnancies That Subsequently Develop Preeclampsia. *Reprod Sci*. 2014;21(6):754–760.

53. Argyraki M, et al. In-utero stress and mode of conception: impact on regulation of imprinted genes, fetal development and future health. *Human Reproduction Update*. 2019;25(6):777–801.

54. Giannoukakis N, et al. Parental genomic imprinting of the human IGF2 gene. *Nat Genet*. 1993;4(1):98–101.

55. Harris LK, et al. IGF2 Actions on Trophoblast in Human Placenta Are Regulated by the Insulin-Like Growth Factor 2 Receptor, Which Can Function as Both a Signaling and Clearance Receptor1. *Biology of Reproduction*. 2011;84(3):440–446.

56. Zeschnigk M, et al. IGF2/H19 hypomethylation in Silver–Russell syndrome and isolated hemihypoplasia. *Eur J Hum Genet*. 2008;16(3):328–334.

57. Maher ER, Reik W. Beckwith-Wiedemann syndrome: imprinting in clusters revisited. *J Clin Invest*. 2000;105(3):247–845.

58. Shukla V, et al. NOTUM-mediated WNT silencing drives extravillous trophoblast cell lineage development. *Proc Natl Acad Sci USA*. 2024;121(40):e2403003121.

59. Stritt S, et al. APOLD1 loss causes endothelial dysfunction involving cell junctions, cytoskeletal architecture, and Weibel-Palade bodies, while disrupting hemostasis. *haematol*. 2022;108(3):772–784.

60. Seguín-Estévez Q, et al. The Transcription Factor RFX Protects MHC Class II Genes against Epigenetic Silencing by DNA Methylation. *The Journal of Immunology*. 2009;183(4):2545–2553.

61. Gobin SJP, et al. The RFX Complex Is Crucial for the Constitutive and CIITA-Mediated Transactivation of MHC Class I and β2-Microglobulin Genes. *Immunity*. 1998;9(4):531–541.

62. Duttaroy A. Transport of fatty acids across the human placenta: A review. *Progress in Lipid Research*. 2009;48(1):52–61.

63. Canton J, Neculai D, Grinstein S. Scavenger receptors in homeostasis and immunity. *Nat Rev Immunol*. 2013;13(9):621–634.

64. Dubé E, et al. Modulation of Fatty Acid Transport and Metabolism by Maternal Obesity in the Human Full-Term Placenta1. *Biology of Reproduction*. 2012;87(1). https://doi.org/10.1095/biolreprod.111.098095.

65. Piechota W, Staszewski A. Reference ranges of lipids and apolipoproteins in pregnancy. *European Journal of Obstetrics & Gynecology and Reproductive Biology*. 1992;45(1):27–35.

66. Sitras V, et al. Differential Placental Gene Expression in Severe Preeclampsia. *Placenta*. 2009;30(5):424–433.

67. Ingman K, et al. Characterisation of Hofbauer Cells in First and Second Trimester Placenta: Incidence, Phenotype, Survival in vitro and Motility. *Placenta*. 2010;31(6):535–544.

68. Tabula Sapiens Consortium*, et al. The Tabula Sapiens: A multiple-organ, single-cell transcriptomic atlas of humans. *Science*. 2022;376(6594):eabl4896.

69. Weakley SM, et al. Expression and Function of a Large Non-coding RNA Gene XIST in Human Cancer. *World j surg*. 2011;35(8):1751–1756.

70. Kim D, et al. Graph-based genome alignment and genotyping with HISAT2 and HISAT-genotype. *Nat Biotechnol*. 2019;37(8):907–915.

71. Pertea M, et al. StringTie enables improved reconstruction of a transcriptome from RNA-seq reads. *Nat Biotechnol*. 2015;33(3):290–295.

72. Heinz S, et al. Simple Combinations of Lineage-Determining Transcription Factors Prime cis-Regulatory Elements Required for Macrophage and B Cell Identities. *Molecular Cell*. 2010;38(4):576–589.

73. Li H, et al. The Sequence Alignment/Map format and SAMtools. *Bioinformatics*. 2009;25(16):2078–2079.

74. Ritchie ME, et al. limma powers differential expression analyses for RNA-sequencing and microarray studies. *Nucleic Acids Research*. 2015;43(7):e47–e47.

75. Zhou Y, et al. Metascape provides a biologist-oriented resource for the analysis of systems-level datasets. *Nat Commun*. 2019;10(1):1523.

76. De Hoon MJL, et al. Open source clustering software. *Bioinformatics*. 2004;20(9):1453–1454.

77. Schnider B, et al. HumanLectome, an update of UniLectin for the annotation and prediction of human lectins. *Nucleic Acids Research*. 2024;52(D1):D1683–D1693.

78. Li H, Durbin R. Fast and accurate short read alignment with Burrows–Wheeler transform. *Bioinformatics*. 2009;25(14):1754–1760.

79. Zhang Y, et al. Model-based Analysis of ChIP-Seq (MACS). *Genome Biol*. 2008;9(9):R137.

80. Amemiya HM, Kundaje A, Boyle AP. The ENCODE Blacklist: Identification of Problematic Regions of the Genome. *Sci Rep*. 2019;9(1):9354.

81. Thorvaldsdottir H, Robinson JT, Mesirov JP. Integrative Genomics Viewer (IGV): high-performance genomics data visualization and exploration. *Briefings in Bioinformatics*. 2013;14(2):178–192.

82. Quinlan AR, Hall IM. BEDTools: a flexible suite of utilities for comparing genomic features. *Bioinformatics*. 2010;26(6):841–842.

83. Saldanha AJ. Java Treeview—extensible visualization of microarray data. *Bioinformatics*. 2004;20(17):3246–3248.

84. Neuperger P, et al. Single-cell mass cytometric analysis of peripheral immunity and multiplex plasma marker profiling of non-small cell lung cancer patients receiving PD-1 targeting immune checkpoint inhibitors in comparison with platinum-based chemotherapy. *Front Immunol*. 2023;14:1243233.

85. Gémes N, et al. Single-cell immunophenotyping revealed the association of CD4+ central and CD4+ effector memory T cells linking exacerbating chronic obstructive pulmonary disease and NSCLC. *Front Immunol*. 2023;14:1297577.

Placenta no.	Gestational age (weeks + days)	Newborn's weight (g)	Umbilical cord pH at delivery	Indication for Elective C-section
Placenta #1	39 + 3	3,420	7.3	Two previous C-sections
Placenta #2	38 + 5	2,640	7.3	Placenta praevia
Placenta #3	39 + 0	3,700	NA	Ophtalmological indication
Placenta #4	39 + 1	3,060	7.4	Ophtalmological indication
Placenta #5	38 + 2	3,600	7.31	Pneumothorax in history

Table 1. Clinical characteristics of placenta donors and indications for elective cesarean section; not applicable (NA)

	Sex of newborn	Weight of collected villous tissue (g)	Number of cells (before immune-purification)	Number of cells per g of fetal villous tissue before immune-purification	Number of CD10 and EGFR double negative cells (after immune-purification)	Number of cells per g of fetal villous tissue after immune-purification	% of $CD163^+$ HBCs in the immune-purified, live cell population
Placenta 1	male	60.20	22x10^7	3.65x10^6	3.0x10^7	0.5x10^6	52.10
Placenta 2	male	72.00	11.52x10^7	1.6x10^6	1.87x10^7	0.26x10^6	81.10
Placenta 3	male	100.80	4.1x10^7	0.41x10^6	2.4x10^7	0.24x10^6	44.20
Placenta 4	female	101.30	22.4x10^7	2.21x10^6	4.15x10^7	0.41x10^6	78.00
Placenta 5	female	147.50	9.9x10^7	0.67x10^6	5.7x10^7	0.39x10^6	70.40

Table 2. Quantitative Analysis of Fetal Villous Tissue and $CD163^+$ Cell Counts in Placentas

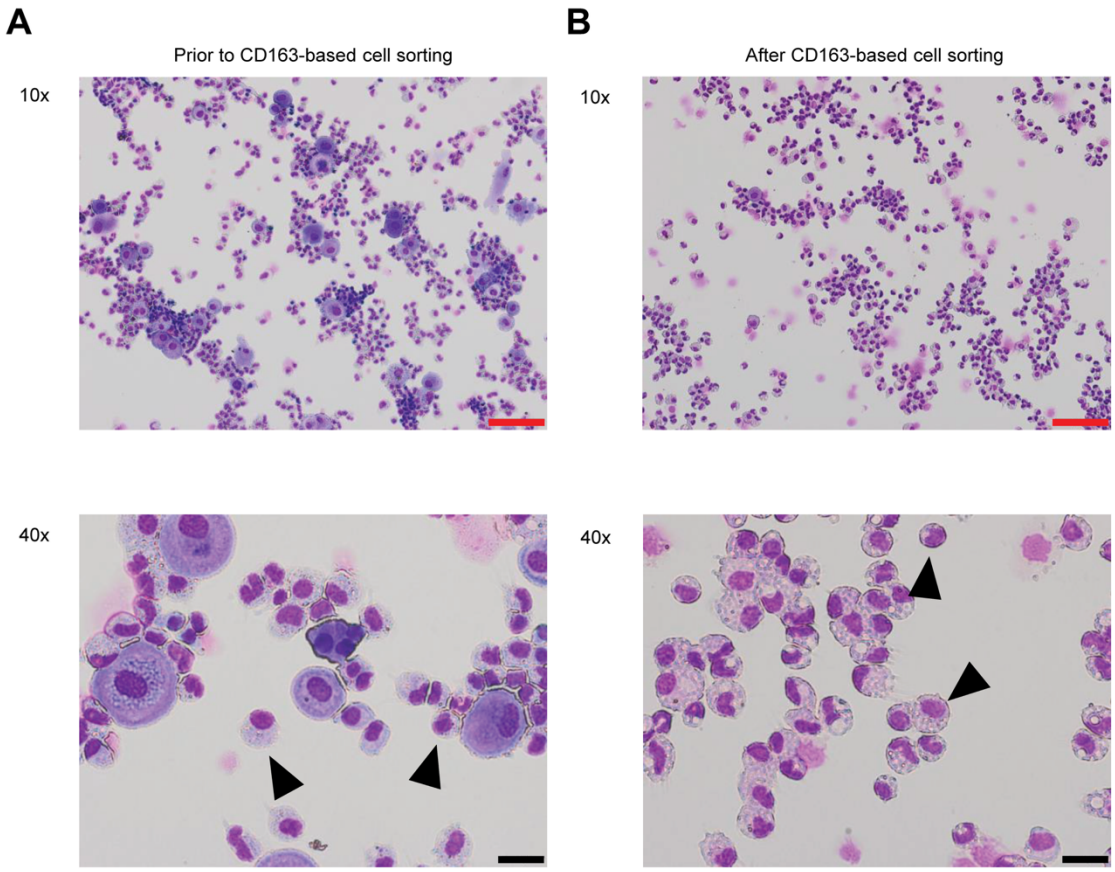

Figure 1. Enrichment of HBCs by CD163-based cell sorting.
Cytospin microscopic pictures showing HBC isolates **(A)** before and **(B)** after CD163-based sorting. Arrowheads point at HBCs. Red scale bars represent 100 μm. Black scale bars represent 20 μm.

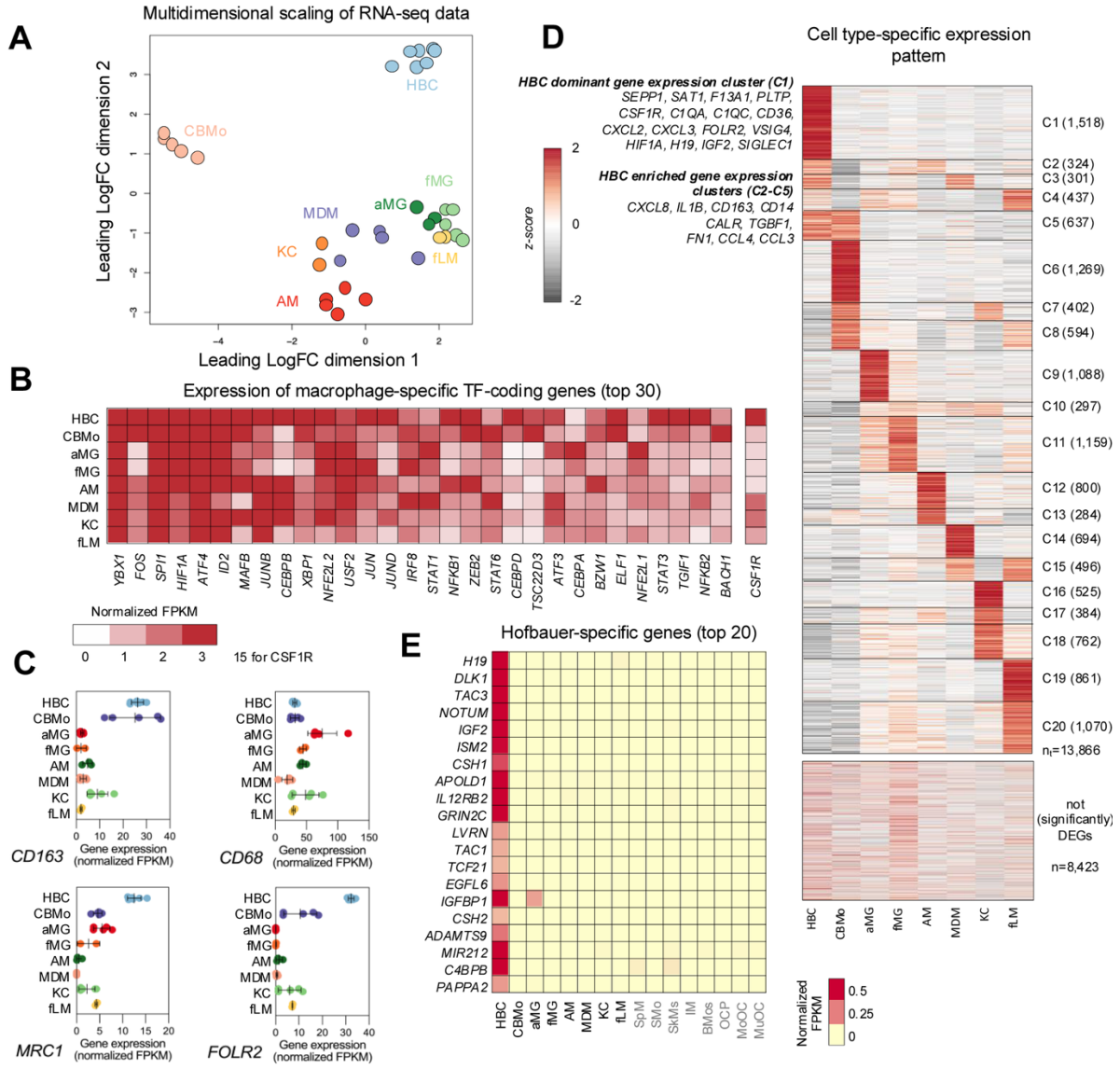

Figure 2. Comparative transcriptomic profiling of HBCs

(A) The multidimensional scaling plot represents the Euclidean distances between the gene expression patterns of the 8 cell types indicated and also between their replicates. **(B)** The heat map shows the average normalized gene expression of the top 30 macrophage-specific TF-coding genes and the CSF1R gene in the 8 cell types. **(C)** Scatter plots showing normalized gene expression values (FPKM) for HBC marker genes, including *CD163*, *CD68*, *MRC1* and *FOLR2* across eight cell types. Points represent individual replicates, with horizontal bars indicating the mean and error bars representing the standard deviation (SD). **(D)** The row-normalized, clustered heat map represents the cell subtype-specific ($p \leq 0.05$; $FD \geq 2$) average of the normalized gene expression patterns and also the non-differentially expressed genes between them. **(E)** The heat map represents the average normalized expression of the top 20 HBC-specific marker genes. The corresponding FPKM scale is shown at the lower left corner of the heat map.

Adult Kupffer cells (KC), monocyte-derived macrophages (MDM), alveolar macrophages (AM), adult microglia (aMG), fetal microglia (fMG), fetal liver macrophages (fLM), mononuclear osteoclasts (MoOCs) and multinucleated osteoclasts (MuOC), osteoclast precursors (OCP), spleen macrophages (SpM), intestinal macrophages (IM), skin macrophages (SkM), spleen monocytes (SMos), blood monocytes (BMo), and cord blood monocytes (CBMo).

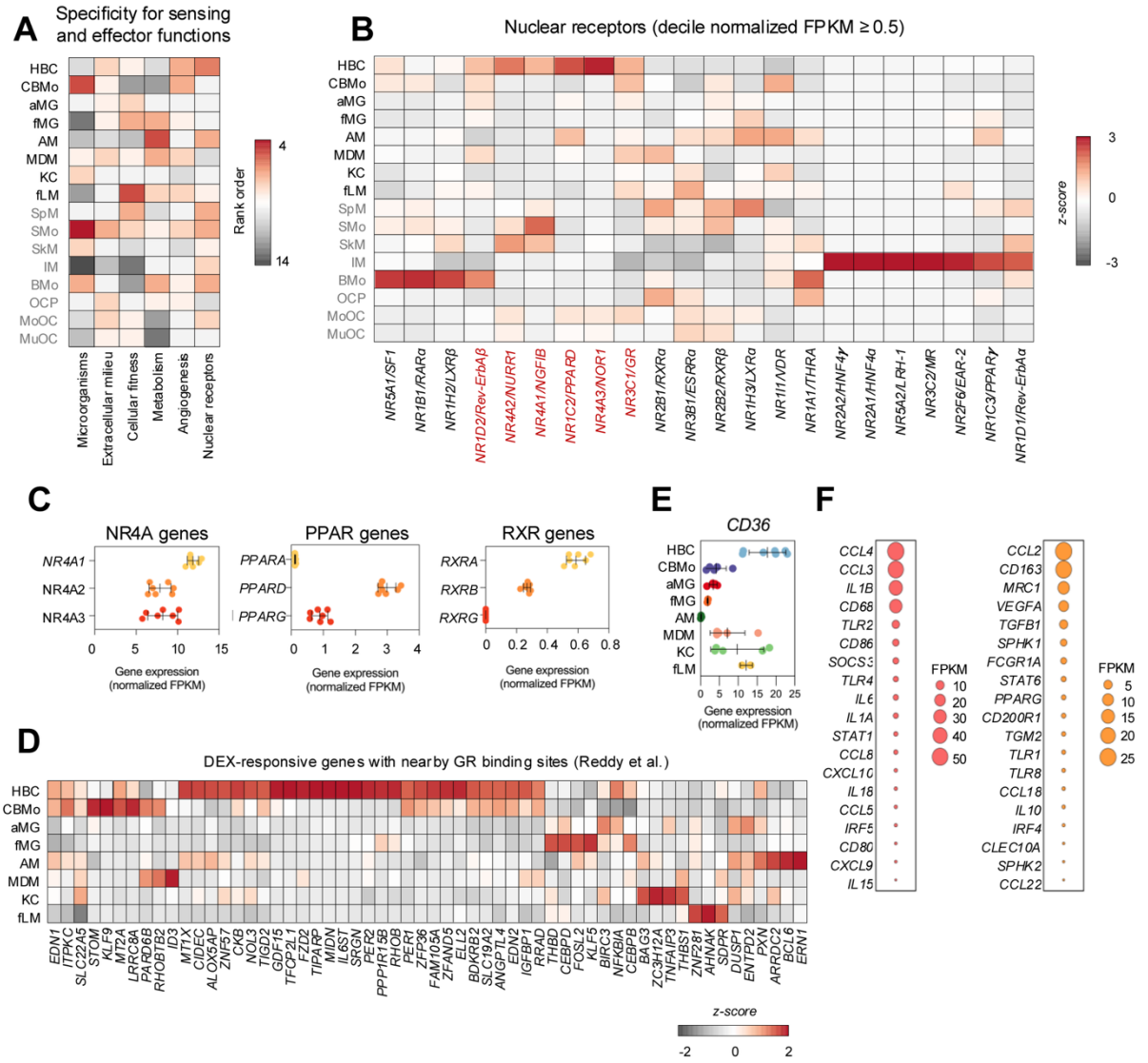

Figure 3. Transcriptional Profiling of Nuclear Receptor Expression and Functional Specificity in the Included Macrophage Populations

(A) The heat map represents the significance of the genes (in rank order) of the 6 highlighted sensing and effector functions in the 16 different cell types. Genes with an expression higher than 0.5 FPKM (after normalization) in any cell type were considered. **(B)** The row-normalized heat map depicts the gene expression of the nuclear receptor superfamily members in the 16 different cell types. **(C)** Scatter plots showing normalized gene expression values (FPKM) for NR4A, PPAR, and RXR family members in sequenced HBC samples. Points represent individual replicates, with horizontal bars indicating the mean and error bars representing the standard deviation (SD). **(D)** The row-normalized heat map depicts the expression of DEX-responsive genes with nearby GR binding sites, which were previously described. (32) **(E)** Scatter plot showing normalized gene expression values (FPKM) of *CD36.* Points represent individual replicates, with horizontal bars indicating the mean and error bars representing the standard deviation (SD). **(F)** Bubble plot shows the expression levels (FPKM) of M1 macrophage marker genes (red, left panel) and M2 macrophage marker genes (orange, right panel) in HBCs. The size of each bubble corresponds to the expression value (FPKM) as indicated in the scale legends. Larger bubbles represent higher transcript abundance.

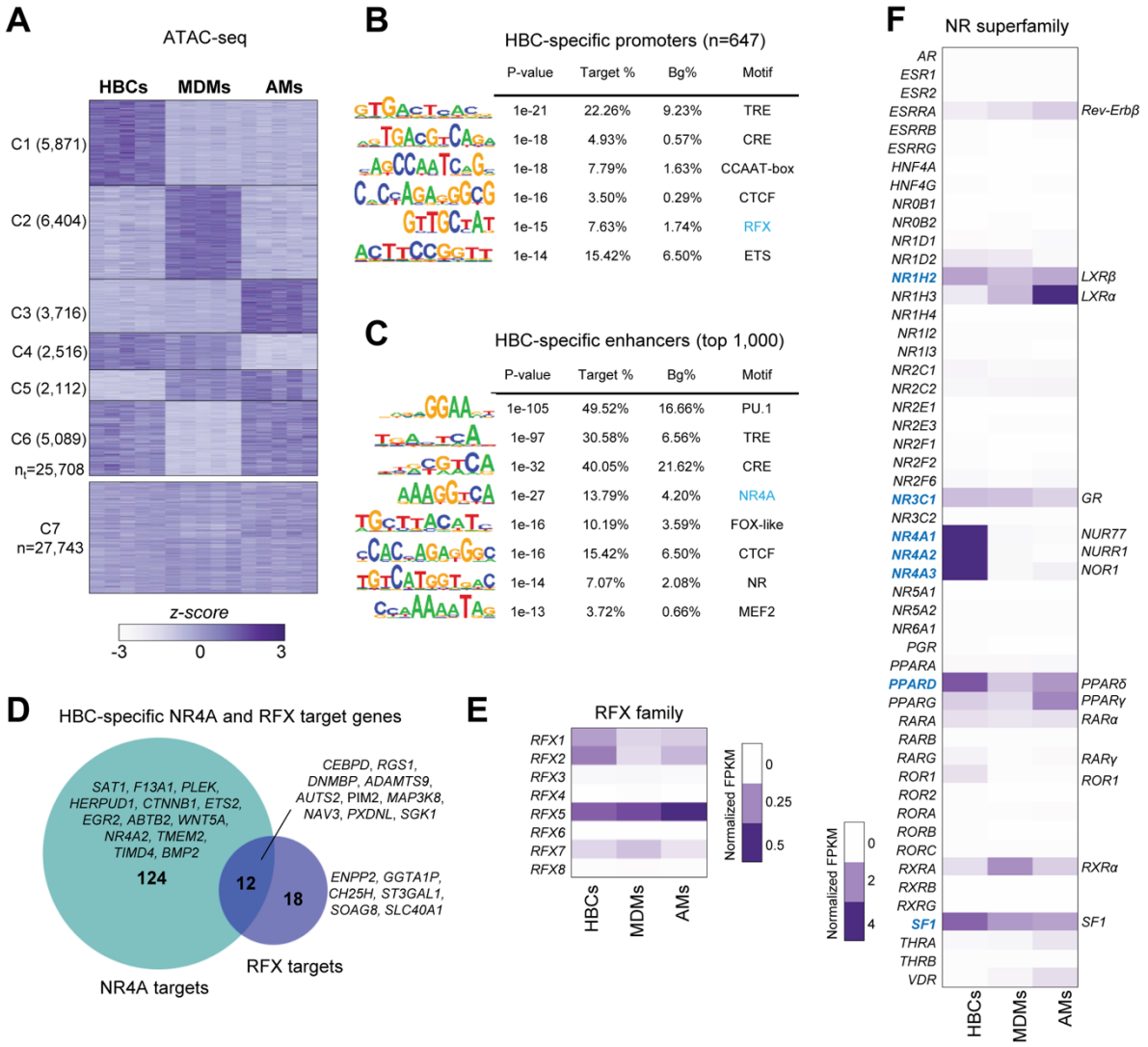

Figure 4. Chromatin accessibility and enrichment of transcription factor motifs delineate HBC-specific regulatory programs

(A) The row-normalized, clustered heat map represents the coverage values of those differentially accessible chromatin regions ($p \leq 0.05$; $FD \geq 2$) specific for the HBCs, MDMs, or AMs, or their combinations (C1-C6). It also depicts the non-differentially accessible chromatin regions (C7). **(B)** The *de novo* motif hits of the HBC-specific TSS-proximal (promoter) (n=647) and **(C)** the top 1,000 TSS-distal (enhancer) regions. Logos of the significantly enriched motifs are presented along with the p-value rank; Bg%: background%. **(D)** The proportional Venn diagram represents the overlap between the NR4A and RFX target genes that display significantly higher expression and where NR4A and RFX motifs are located within more accessible chromatin regions in HBCs. The heat maps represent **(E)** the average normalized gene expression of the members of the *RFX* and **(F)** the nuclear receptor (super)families in the HBCs, MDMs, or AMs. The row-normalized heat map represents the coverage values.

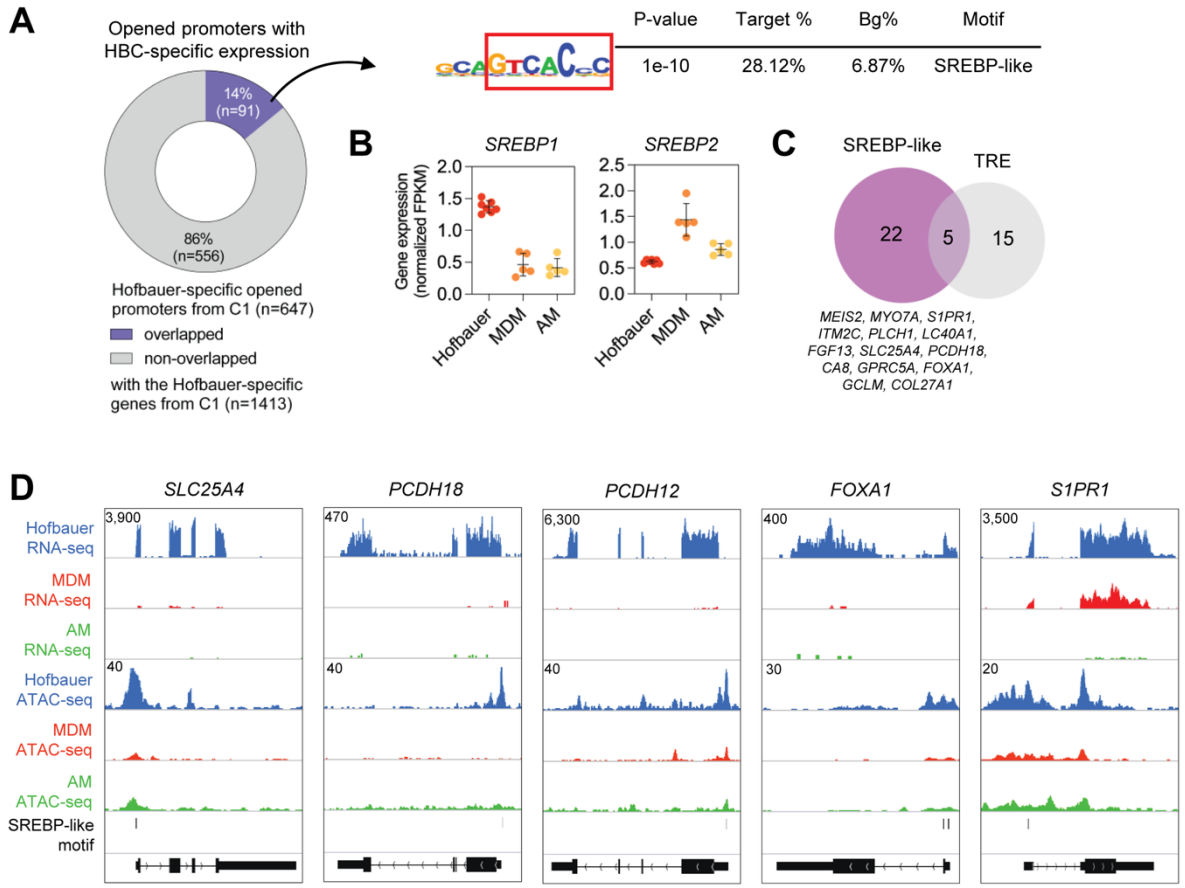

Figure 5. SREBP-like Motif Enrichment and Target Gene Activity in HBCs
(A) SREBP-like motif enriched in promoters of genes that are upregulated and have more increased promoter accessibility in HBCs. **(B)** Gene expression of the SREBP1 and SREBP2 genes in HBCs, MDMs, and AMs. **(C)** Number of mapped SREBP-like and TRE motifs in open promoters of 91 HBC-specific genes. Selected genes with SREBP-like motifs are highlighted. **(D)** The genome browser view of RNA- and ATAC-seq coverages of HBC, MDM, and AM cells on the SLC25A4, PCDH18, PCDH12, FOXA1 and S1PR1 loci. The coverage files of the replicates are overlayed, and the interval scales are highlighted in all cases.

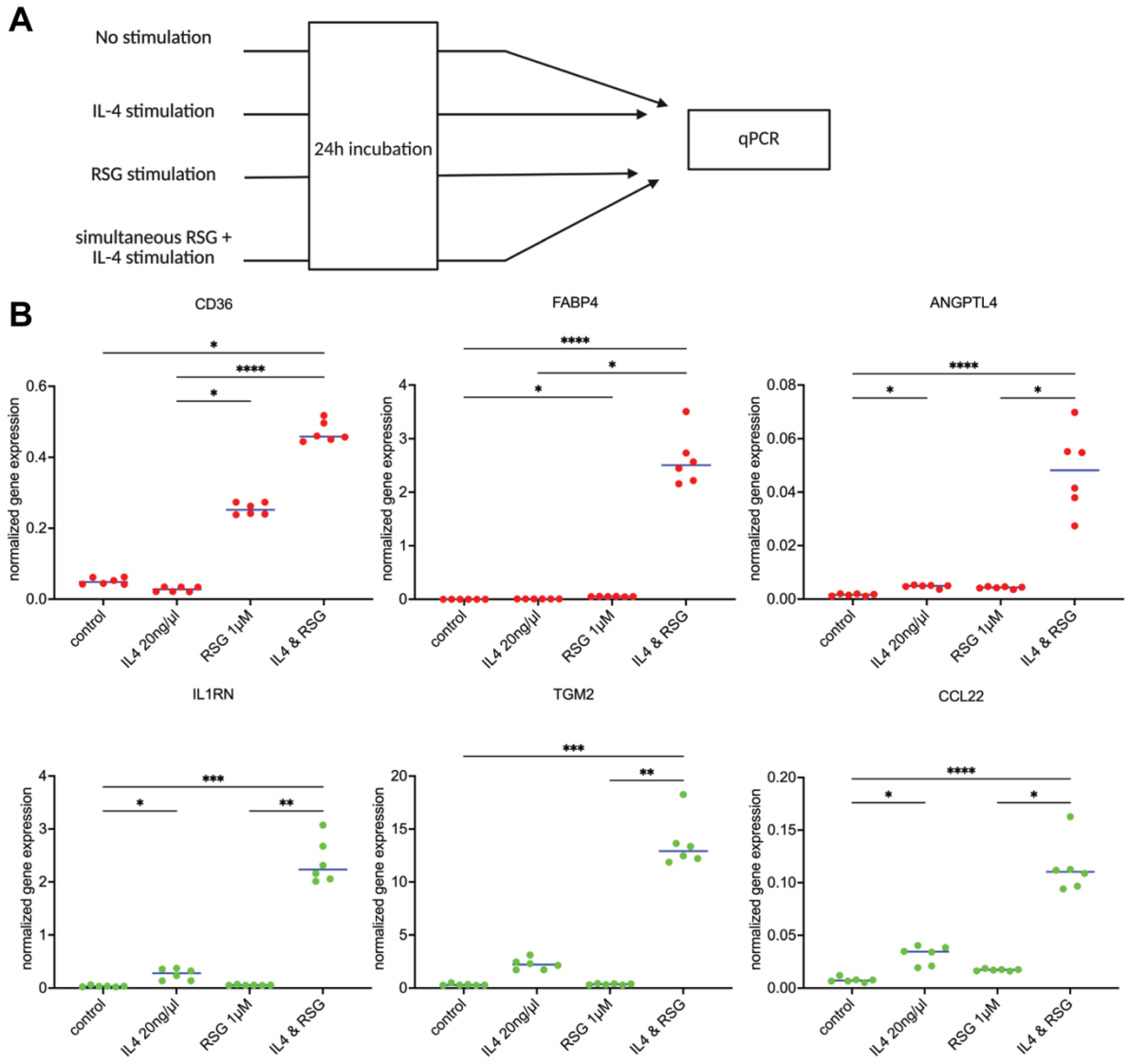

Figure 6. Synergistic effects of RSG and IL-4 on gene expression in *in vitro* stimulation assays

(A) Experimental outline of the *in vitro* induction studies. **(B)** Normalized mRNA expression levels after *in vitro* RSG and IL-4 induction, measured using PCR. Canonical PPARγ target genes are in red, and IL-4-induced genes are in green. Blue lines represent the medians of individual values. Pairwise comparisons were made using Kruskal-Wallis tests followed by Dunn's post hoc tests. The figure depicts replicates from the cells of the same placenta (placenta number 5). 1 dot represents 1 parallel measurement. Canonical PPAR*γ* target genes are indicated in red, canonical IL-4-induced genes are indicated in green.
Statistical significance is indicated as follows: $p < 0.05$ (*), $p < 0.01$ (**), $p < 0.001$ (***), $p < 0.0001$ (****). Supplementary Figure 9 depicts the PCR data of 4 placentas.

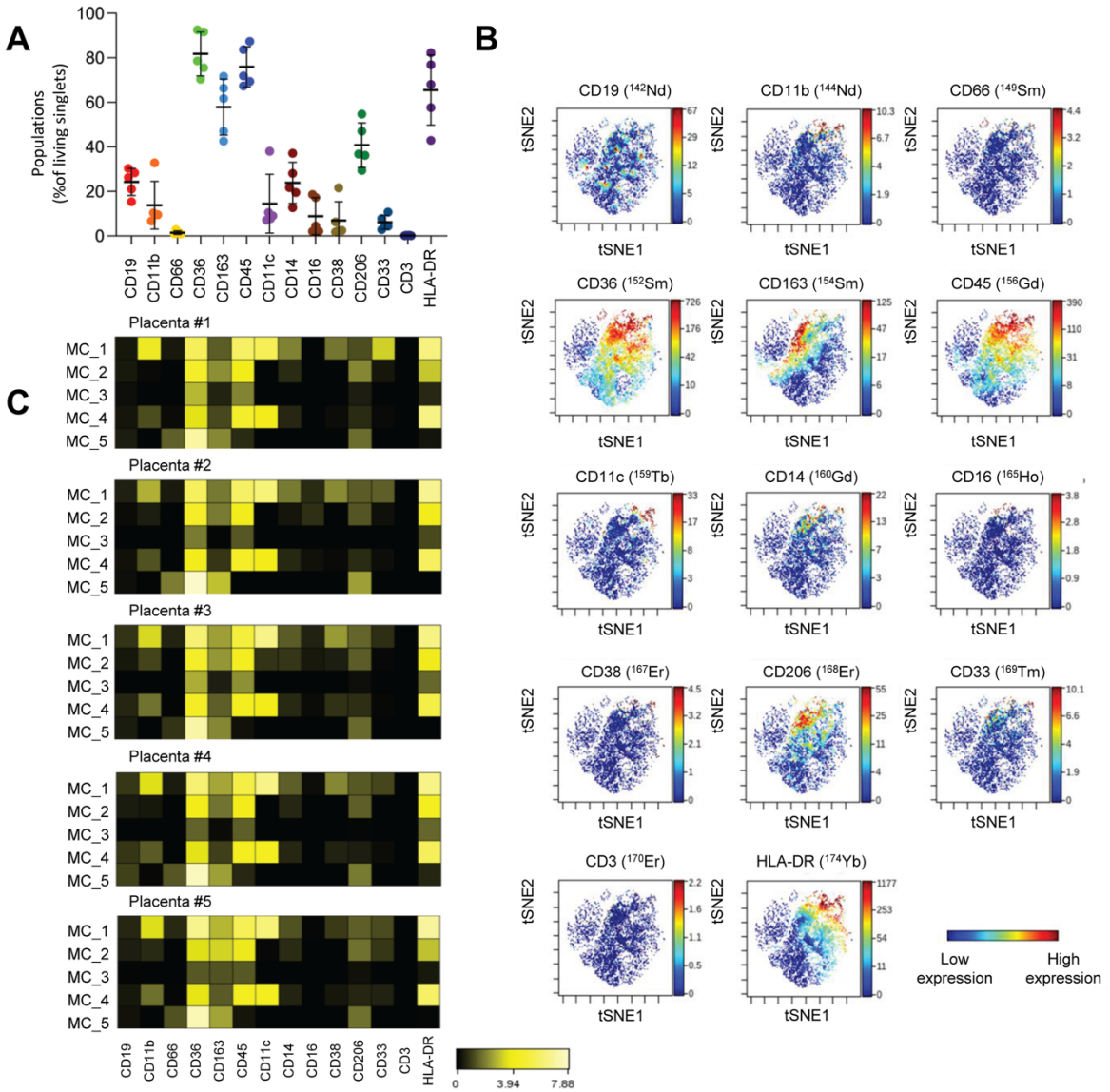

Figure 7. Single-cell heterogeneity of HBCs revealed by multidimensional immunophenotyping using CyTOF.

(**A**) The percentage of HBCs (n=5) for the expression of the investigated 14 markers in relation to the living singlets. (**B**) The viSNE (visualization of stochastic neighbor embedding) analysis of HBCs, 8,500 cells per sample were viSNE plotted in Cytobank within the living singlets according to the following parameters: iterations: 1,000, perplexity: 30, theta: 0.5. Blue corresponds to low expression; red corresponds to high expression. (**C**) Comparative heatmap (table's minimum setting in Cytobank) of mass cytometry data (arcsinh-transformed median intensity values; shown on the color scale) regarding marker expression intensity values of the FlowSOM metaclusters.